Copyright Warning & Restrictions

The copyright law of the United States (Title 17, United States Code) governs the making of photocopies or other reproductions of copyrighted material.

Under certain conditions specified in the law, libraries and archives are authorized to furnish a photocopy or other reproduction. One of these specified conditions is that the photocopy or reproduction is not to be "used for any purpose other than private study, scholarship, or research." If a, user makes a request for, or later uses, a photocopy or reproduction for purposes in excess of "fair use" that user may be liable for copyright infringement,

This institution reserves the right to refuse to accept a copying order if, in its judgment, fulfillment of the order would involve violation of copyright law.

Please Note: The author retains the copyright while the New Jersey Institute of Technology reserves the right to distribute this thesis or dissertation

Printing note: If you do not wish to print this page, then select "Pages from: first page # to: last page #" on the print dialog screen

ABSTRACT

DENOISING TECHNIQUES REVEAL NEURAL CORRELATES OF MODULATION MASKING RELEASE IN AUDITORY CORTEX

By
Sahil Chaubal

Hearing aids allow hearing impaired (HI) individuals to regain auditory perception in quiet settings. However, despite advances in hearing aid technology, HI individuals do not perform as well in situations with background sound as normally hearing (NH) listeners. An extensive literature demonstrates that when comparing tone detection performance in background noise, NH listeners have better thresholds when that noise is temporally modulated as compared to temporally unmodulated. However, this perceptual benefit, called Modulation Masking Release (MMR), is much reduced in HI listeners, and this is thought to be a reason for why HI listeners struggle in the presence of background sound.

This study explores neural correlates of MMR in NH and HI gerbils. Trained, awake gerbils (Meriones unguiculatus) listen passively to a target tone (1 kHz) embedded in modulated or unmodulated noise while a 16-channel microelectrode array records multi-unit neural spike activity in core auditory cortex. In addition, microelectrodes also record nuisance signals due to animal movements and interference in the wireless recording setup. The current study examines the potency of three different denoising algorithms using signal detection theory. The first, amplitude rejection (AR) classifies events based on amplitude. The second, virtual referencing (VR) applies subtraction of a virtual common ground signal. The third, inter-electrode correlation (IEC) compares events across electrodes to decide whether to classify an event as noise or as spike. Using Receiver-Operator-Characteristics (ROC), these classifiers were ranked. Results suggest that combining IEC

and VR leads to best denoising performance. Denoised spike train reveals a robust correlation of spike rate with behavioral performance. Results hint that neural correlates of MMR are not primarily based on spike rate coding, at least in the core auditory cortex.

DENOISING TECHNIQUES REVEAL NEURAL CORRELATES OF MODULATION MASKING RELEASE IN AUDITORY CORTEX

by
Sahil Chaubal

A Thesis
Submitted to the Faculty of
New Jersey Institute of Technology,
The State University of New Jersey - Newark
in Partial Fulfillment of the Requirements for the Degree of
Master of Science in Biomedical Engineering

Department of Biomedical Engineering

January 2017

APPROVAL PAGE

DENOISING TECHNIQUES REVEAL NEURAL CORRELATES OF MODULATION MASKING RELEASE IN AUDITORY CORTEX

Sahil Chaubal

Dr. Antje Ihlefeld, Thesis Advisor — Date
Assistant Professor of Biomedical Engineering, NJIT

Dr. Richard A. Foulds, Committee Member — Date
Associate Professor of Biomedical Engineering, NJIT

Dr. Mesut Sahin, Committee Member — Date
Professor of Biomedical Engineering, NJIT

Dr. Xiaobo Li, Committee Member — Date
Associate Professor of Biomedical Engineering, NJIT

BIOGRAPHICAL SKETCH

Author: Sahil Chaubal

Degree: Masters of Science

Date: January 2017

Undergraduate and Graduate Education:

- Masters in Biomedical Engineering,
  New Jersey Institute of Technology, Newark, NJ, 2017

- Bachelor of Science in Biomedical Engineering,
  Mumbai University, Mumbai, India, 2013

Major: Biomedical Engineering

"You are the creator of your own destiny"

This thesis is dedicated to my Mother's love and her unyielding belief, Father's support and guidance, and Grandparent's blessings. This feat wouldn't have be possible without your relentless motivation.

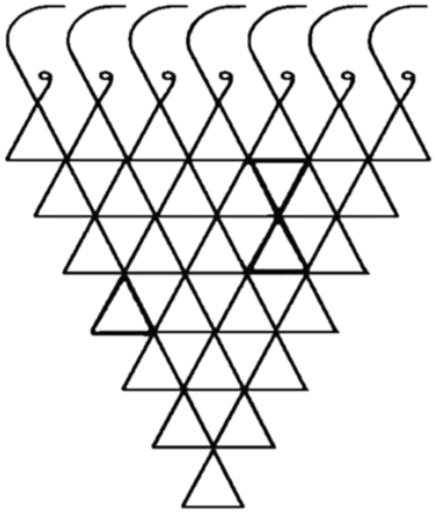

ACKNOWLEDGMENT

My deepest gratitude to Dr. Antje Ihlefeld, who guided me throughout this research with her valuable time and assistance, without which the accomplishment of the task would have never been possible. Dr. Ihlefeld's constant encouragement towards learning and engagement through this learning process has helped me a lot to cope up in this thesis.

I also thank Dr. Richard Foulds for being in my committee and being my mentor for the MATLAB course, without it working on programming for this thesis work would have been very difficult.

I am equally thankful to Dr. Mesut Sahin and Dr. Xiaobo Li for taking out their valuable time in reviewing my work and actively participating in my committee.

Lastly, I thank my colleagues and friends in Neural Engineering Speech and Hearing Laboratory, Nima Alamatsaz, Min Zhang and Joshua Hajicek for continuous support and assistance.

TABLE OF CONTENTS

TABLE OF CONTENTS
(Continued)

Chapter **Page**

LIST OF TABLES

LIST OF FIGURES

LIST OF FIGURES
(Continued)

Figure **Page**

LIST OF FIGURES
(Continued)

Figure **Page**

LIST OF DEFINITIONS

AR	Amplitude Rejection
AR_{NoV}	Amplitude rejection without Virtual referencing
AR_{VR}	Amplitude rejection with Virtual referencing
AUC	Area Under Curve
dB	Decibel
HI	Hearing Impaired
IEC	Inter-Electrode Correlation
IEC_{NoVR}	Inter-Electrode correlation without Virtual referencing
IEC_{VR}	Inter-Electrode correlation with Virtual referencing
Kp	Kneepoint
M2	Unmodulated on-target Noise Stimuli
M4	Modulated on-target Noise Stimuli
MMR	Modulation Masking Release
NH	Normal Hearing
$p_{onetailed}$	Onetailed P-value
ROC	Receiver Operative Characteristics
SD	Standard Deviation.
SPL	Sound Pressure Level
TMR	Target Masker Ratio
VR	Virtual Referencing

CHAPTER 1

INTRODUCTION

Most hearing impaired (HI) listeners can detect and identify sound cues in a quiet environment, but struggle to hear when background sound masks these cues. The ability to detect sound cues depends on the nature of the masking sound. Specifically, maskers may be temporally stationary (unmodulated) or fluctuating (modulated). Target detection performance for these maskers generally improves with increasing signal-to-noise energy ratio between target and maskers. Furthermore, tone detection performance is generally better with a modulated masker when compared with an unmodulated masker. One possible strategy that listeners may utilize in modulated background sound is to listen in the energetic dips of the masker where the SNR is high. Indeed, Normal Hearing (NH) listeners can take advantage of dips of the time-varying noise and "listen in the dips" of fluctuating background noise (masking) to extract information from the target signal, a process termed a "dip-listening" (Jin et al., 2010, Ihlefeld et al., 2012) (Figure 1.1).

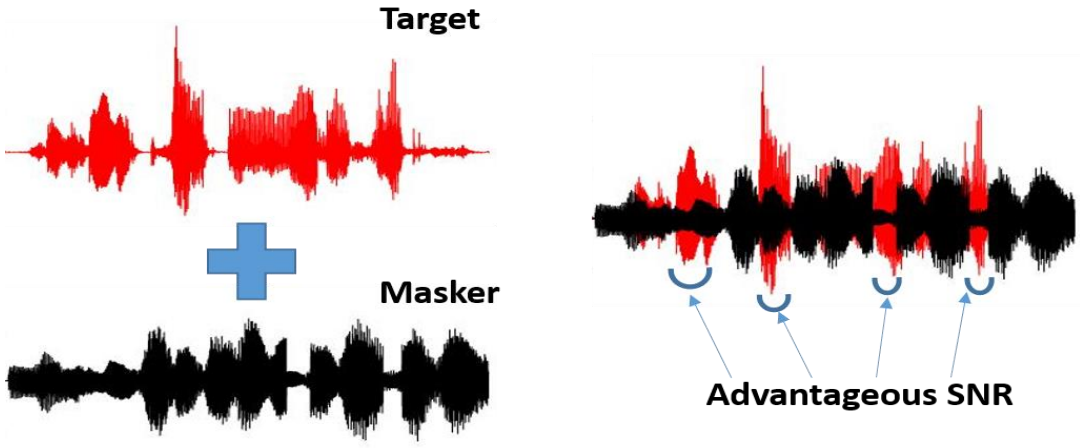

Figure 1.1 Dip-Listening. When the sound cues (target in red) and fluctuating background noise (masker in black) are heard at the same time, normal hearing listeners can extract target information during the dips (pointed arrows) of the masker, this is called dip-Listening.

Auditory sensitivity declines for NH and HI listeners in noisy environments, through masking, but it can improve when this masker level fluctuates, a phenomenon referred to as masking release (Hall et al., 1994, review: Verhey et al., 2003). A common test of masking release presents a target tone in the presence of a narrowband noise that is centered at the target frequency. There is an improved performance in tone detection with modulated masker as compared to unmodulated masker. This improved performance can be further enhanced by adding a band of noise (flanking band), which is spectrally remote from the target signal on the frequency spectrum (Figure 1.2). The flanking band must be coherently modulated with the Modulated and the unmodulated on-target masker. This perceptual benefit is called Modulation Masking Release (MMR).

Previous studies show that along with humans there are other species which can benefit from MMR (Goense and Feng, 2012, Gleich et al., 2007). For example, Mongolian gerbils (Meriones unguiculatus) can benefit from MMR (Wagner 2002; Gleich et al., 2007), and are a suitable model for studying the effect of hearing loss.

To study the effect of MMR in the central auditory system, neural recordings from auditory cortex of NH and HI gerbils were obtained during target detection in MMR condition at different sound intensities (dB SPL). Intracortical microelectrode arrays offer the spatial and temporal resolution to record spike activity (Schwartz AB, 2006). Specifically, the electrical activity is measured over a population of neurons by placing one or more electrodes that are closely spaced into the core auditory cortex and a ground electrode that is some distance away from the recording electrodes. Once electrodes are implanted, they record neural activity in a discrete brain area by transducing extracellular spike activity into voltage signals that are amplified and stored for further analysis.

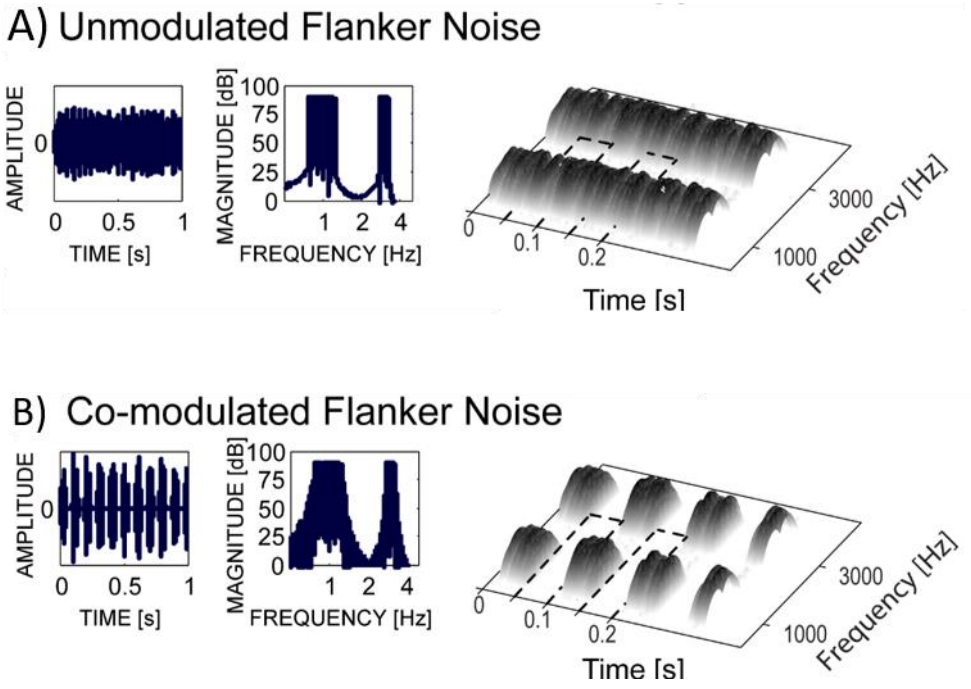

Figure 1.2 Stimulus Design. A) Unmodulated on-target noise. B) Modulated on-target noise.
Source: Antje Ihlefeld, Yi Wen Chen, Dan H. Sanes. (2016). Developmental Conductive Hearing Loss Reduces Modulation Masking release.

These electrodes were positioned in the left auditory cortex with ground wire was inserted contralaterally. A 16-channel wireless headstage and receiver was used in conjunction with a preamplifier and analog-to-digital converter (Buran, von Trapp, & Sanes, 2014) (Figure 1.3). Example voltage traces of the recorded electrophysiological signals are shown in Figure 1.4.

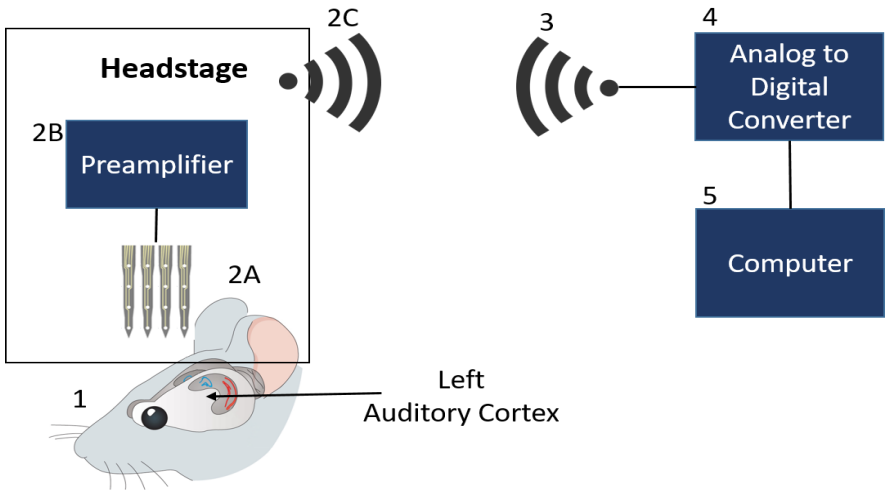

Figure 1.3 Experiment Block Diagram. In this experiment, Microelectrodes (2A) are inserted in the left auditory cortex of Gerbil (1). The neural activity received in the form of voltage is preamplified (2B) and transmitted wirelessly (2C).At the receiver (3) the signal received is digitized at Analog to digital converter (4) and sent to the computer (5) where the electrophysiological signal (Figure 1.4) is viewed.

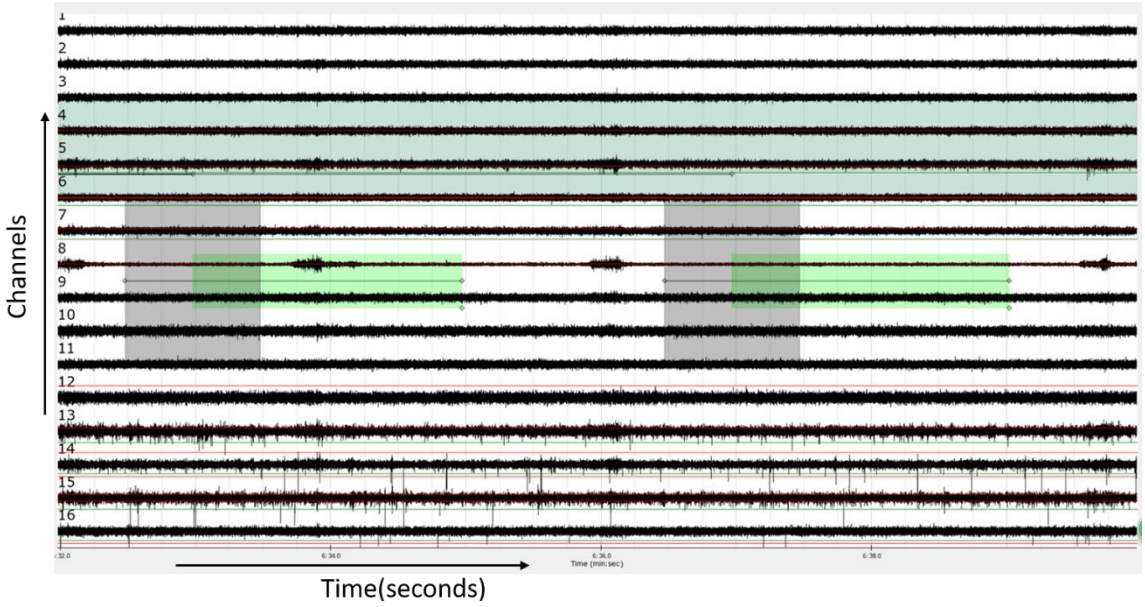

Figure 1.4 The electrophysiology signal from 16 electrodes after multi-unit study. The voltage traces received from the auditory cortex of the Gerbil in trials of different masker type. The above figure shows two trials without the presence of common noise (uncontaminated), the experienced researcher marks such trials as “uncontaminated” trials.

During recordings, animals were awake and non-restrained inside the recording cage. As animals groom, chew and accidently bang against the cage structure, these physical movements cause addition of nuisance signals to the desired neural discharge. Therefore, in addition to multi-unit neural spike activity, microelectrodes also record electromyographic activity (EMG) from muscles, especially mastication signals, and relatively large signals generated by abrupt animal movements, or interference with the recording setup (Gilmour et al., 2006, Paralikar et al., 2009). This adds nuisance noise to the signal. These non-neural nuisance signals have similar spectral and temporal characteristics as the desired neural signals, complicating the detection of neural spikes.

To get a first order approximation, this nuisance noise should present in all recording electrodes and is thus referred to as common noise. Those trials during a recording session where common noise was presented are referred to as *contaminated trials*. When the combined voltage of neural spikes and common noise exceeds the threshold defined by a criterion respective of the channel, it is referred to as a spike event. Spike-detection schemes that involve threshold-based neural spike detection on an electrode by electrode basis may suffer from high false-positive detection due to the presence of common noise, thereby negatively impacting spike-sorting operations.

In this study, we tested how three different classifiers performed for eliminating these recording artifacts. Specifically, these classifiers were compared and ranked using signal detection theory. We then used the best classifier to denoise the data. Analyzing the clean data reveals a modest correlation between mean neural firing rate in auditory cortex and behavioral sensitivity.

CHAPTER 2

BACKGROUND

2.1 Modulation Masking Release

A recent study by Ihlefeld et al. measured behavioral threshold for tone detection for NH and HI gerbils. The ability to detect a tone in a background of modulated or unmodulated masking nose at different sound intensity level (TMR-target masker ratio) was measured, and the percent correct scores were fit by logistic psychometric function (Ihlefeld et al., 2016). The results were converted into d' (d-prime) scores, by calculating the difference in z-scores of hit rate versus false alarm rate, to correct for the bias (Klein, 2001).

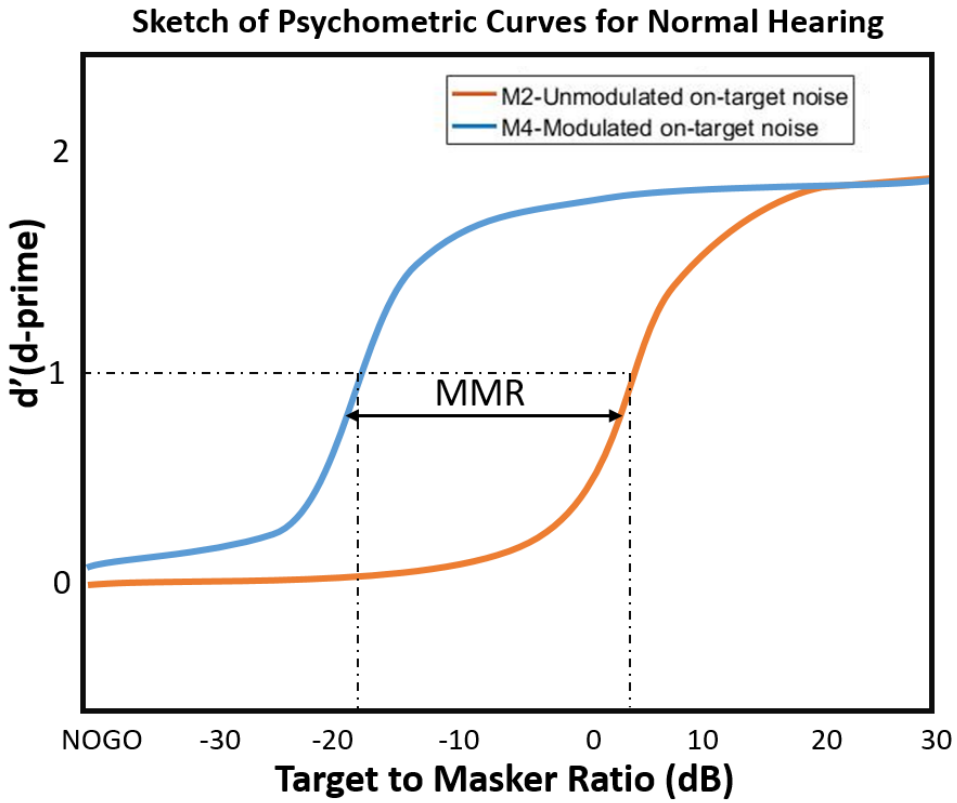

Figure 2.1 Sketch of psychometric curves for Normal Hearing animals. Redrawn from the fitted psychometric curves derived in this study.
Source: Developmental Conductive Hearing Loss Reduces Modulation Masking release, Antje Ihlefeld, Yi Wen Chen, Dan H. Sanes. (2016).

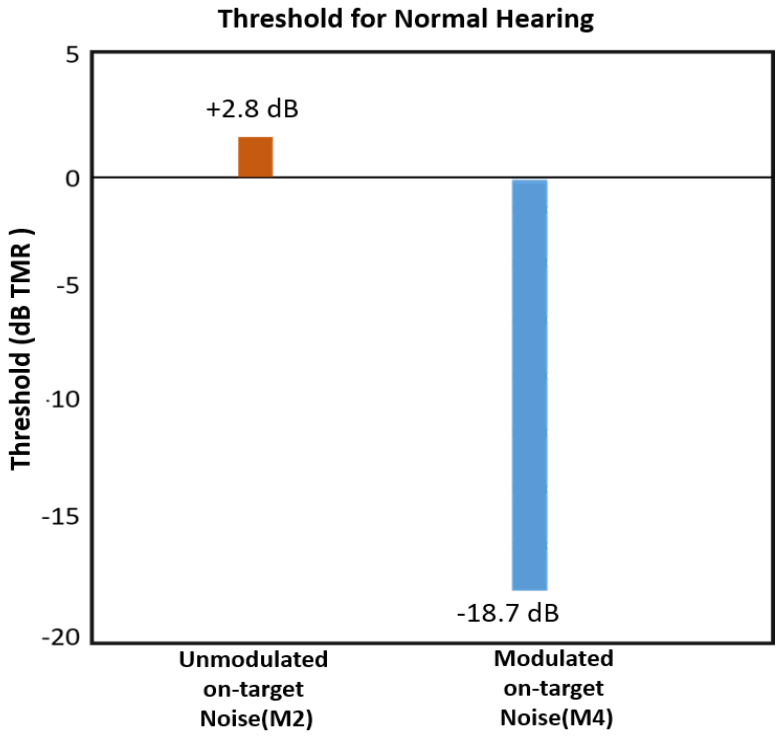

Figure 2.2 Threshold for Normal Hearing at both masker condition at d'=1.
Source: Plotted from data derived in Developmental Conductive Hearing Loss Reduces Modulation Masking release, Antje Ihlefeld, Yi Wen Chen, Dan H. Sanes. (2016).

On plotting the psychometric function, a TMR value corresponding to d'=1 are the TMR threshold values for their respective masker type (Figure 2.1 and Figure 2.3). The difference in the TMR threshold values of modulated and unmodulated noise is called the masking release.

The above study for NH gerbils showed that at d'=1 the TMR threshold for Modulated on-target noise (M4) is -18.7 dB TMR and for Unmodulated on-target noise (M2) is +2.8 dB TMR (Figure 2.2). The masking release i.e. the difference in the Modulated and Unmodulated masker threshold is called the Modulation Masking Release (MMR) which is 21 dB TMR. Similarly, for HI Gerbils their TMR threshold in tone detection during Modulated masker is at 0.11 dB TMR and during Unmodulated masker is +3.8 dB TMR (Figure 2.4). The MMR for HI is 3.7 dB TMR which is very less than the

NH Gerbil. When comparing the TMR threshold during Modulated masker for NH and HI, it shows that the TMR threshold level for HI decreases by 18.5 dB, which indicates that sound deprivation can reduce the ability to listen in the dips of a fluctuating background noise (Modulated Masker). The goal of the current study is to look whether the neural correlates of MMR responds according to the above psychometric functions.

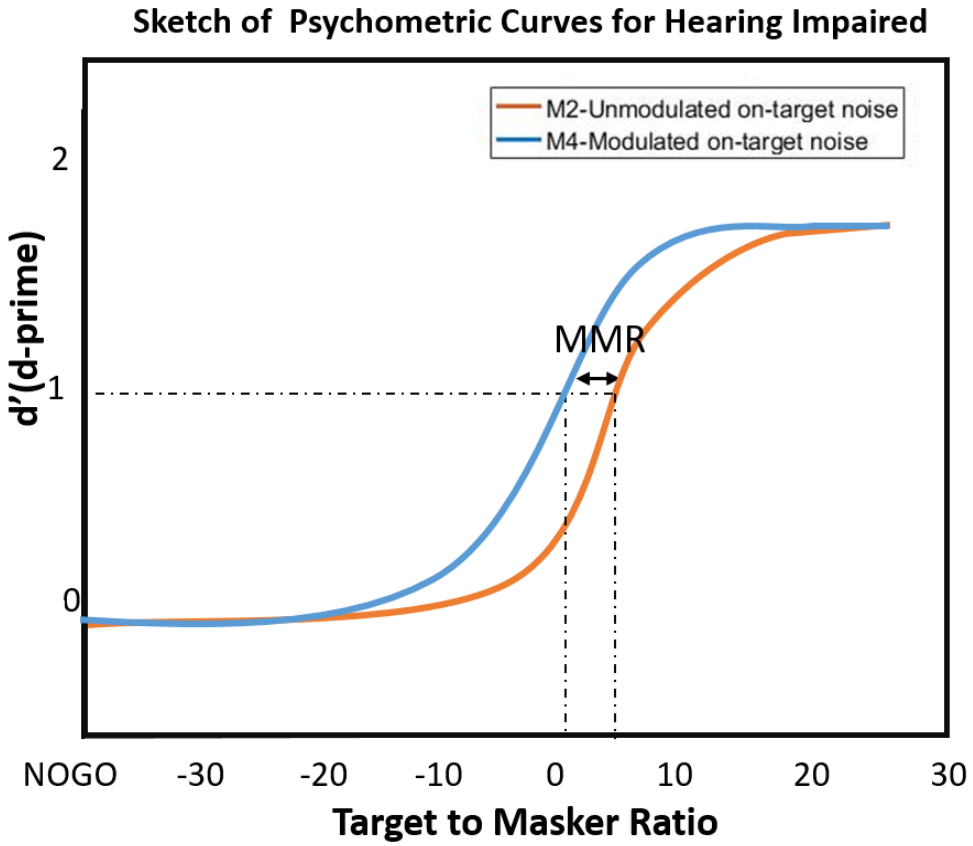

Figure 2.3 Sketch of psychometric curves for Hearing Impaired animals. Redrawn from the fitted psychometric curves derived in this study.
Source: Developmental Conductive Hearing Loss Reduces Modulation Masking release, Antje Ihlefeld, Yi Wen Chen, Dan H. Sanes. (2016).

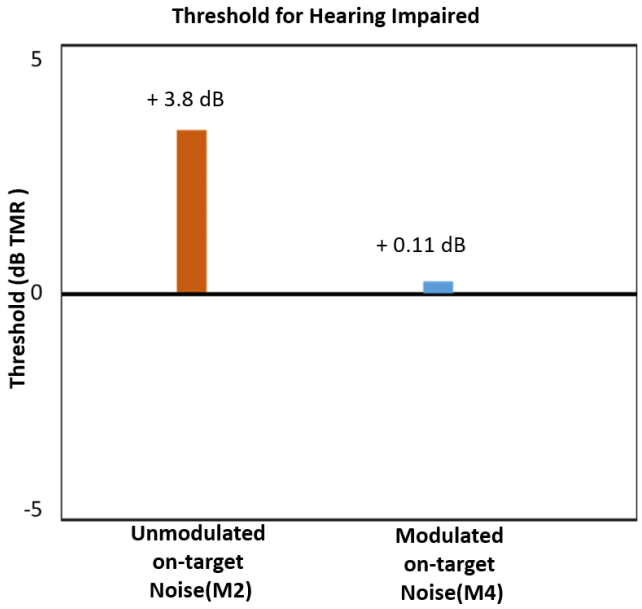

Figure 2.4 Threshold for Hearing Impaired at both masker condition at d'=1.
Source: Plotted from data derived in Developmental Conductive Hearing Loss Reduces Modulation Masking release, Antje Ihlefeld, Yi Wen Chen, Dan H. Sanes. (2016).

2.2 Receiver Operating Characteristics

Signal detection theory provides a precise language and graphic notation for analyzing decision making in the presence of uncertainty. To simplify the decision making outcomes across all possible criteria, the receiver operating characteristic (ROC) curve is used. The ROC curve is a graphical plot of how often false positive (x-axis) occur versus how often true positive (y-axis) occur for different criterion level. The advantage of ROC curves is that they can fully characterize both sensitivity and bias of a decision algorithm in one graph.

ROC curves can also be used to compare the performance of two or more algorithms. The ROC curve is a fundamental tool of signal detection theory for evaluating the performance of classifiers. Figure 2.5 shows the probability density distributions of two populations, one population with contaminated trials, and the other population with uncontaminated trials. These events are classified as either spike or artefact. As in the

example, where the two probability distribution overlap, a perfect separation between the two groups rarely occurs. However, an ideal and unbiased decision making strategy places criterion at the intersection between the probability densities (Wickens, 2001).

There are two main components to the decision-making process: information acquisition and criterion selection.

2.1.1 Criterion Selection (Predicted Condition)

The criterion on the probability distribution graph divides the graph into four sections that correspond to: True positive (TP), False positive (FP), False negative (FN) and True negative (TN).

For every changing criterion to discriminate between the two populations, there will be some cases in which the contaminated trials are correctly identified by the classifier as artefact. These trials are called True Positive. However, other trials where artefacts were present but which the classifier labels non-contaminated trials are termed as False Negative. Those uncontaminated trials that the classifier correctly identified are called True Negative. Trials that the classifier labels as artefacts even though only neural events were present are referred to as False Positive as shown in Figures 2.5 and 2.6.

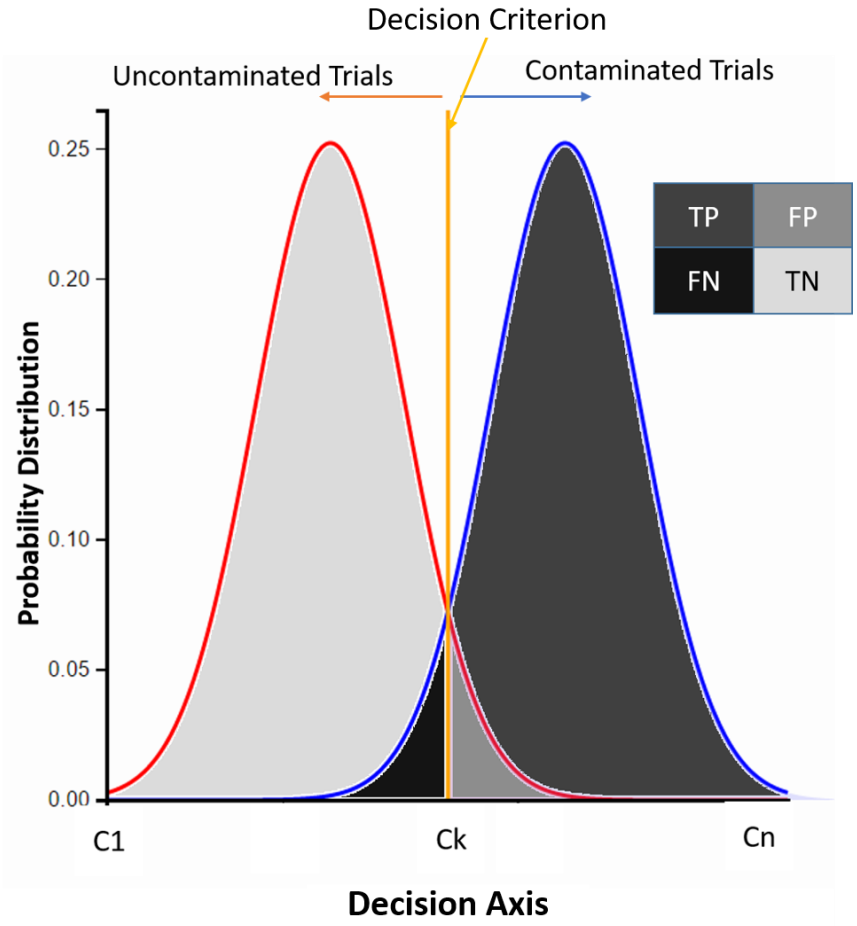

Figure 2.5 Distribution for ROC analysis. The contaminated trial distribution on the right and uncontaminated trial distribution on the left. Moving the criterion value (yellow line) (In our study the standard deviation for AR and number of channels for IEC) step by step will give a point of perfect separation (least possible overlap) between these distributions. TN: True Negative. FN: False Negative. FP: False Positive. TP: True Positive.

		True Condition Positive	True Condition Negative
		Ground Truth Artefact Present	Ground Truth Artefact Absent
Predicted Condition Positive	Algorithm Artefact Present	True Positive	False Positive
Predicted Condition Negative	Algorithm Artefact Absent	False Negative	True Negative

Figure 2.6 ROC Comparison matrix.

True positive and true negative are good, false positive and false negative are bad for the performance of the classifier. Using these four outcomes, the true positive rate and false positive rate is derived.

$$\text{False Positive Rate} = \frac{\text{False Positive}}{\text{False Positive} + \text{True Negative}} \tag{2.1}$$

$$\text{True Positive Rate} = \frac{\text{True Positive}}{\text{True Positive} + \text{False Negative}} \tag{2.2}$$

2.1.2 Information Acquisition(True Condition)

An important component in describing a classification algorithm is the acquisition of ground truth data. Ground truth is reliable information about trial being contaminated or not. Here, an experienced reseacher derived the ground truth by visually inpecting every trial of the datasets. The researcher marked all the trials as “contaminated trials” which appeared to have common noise due to characteristic temporal patterns commonly associated with animal movement which would be seen in all the channels or whose signal amplitude was unusually high compared to median amplitude of the recordings

This truth condition decision is made on the basis of common noise present in all of the channels. One of the example, in which there is a pressence of common noise, is shown in the Figure 2.7 where it is termed as contaminated trial.

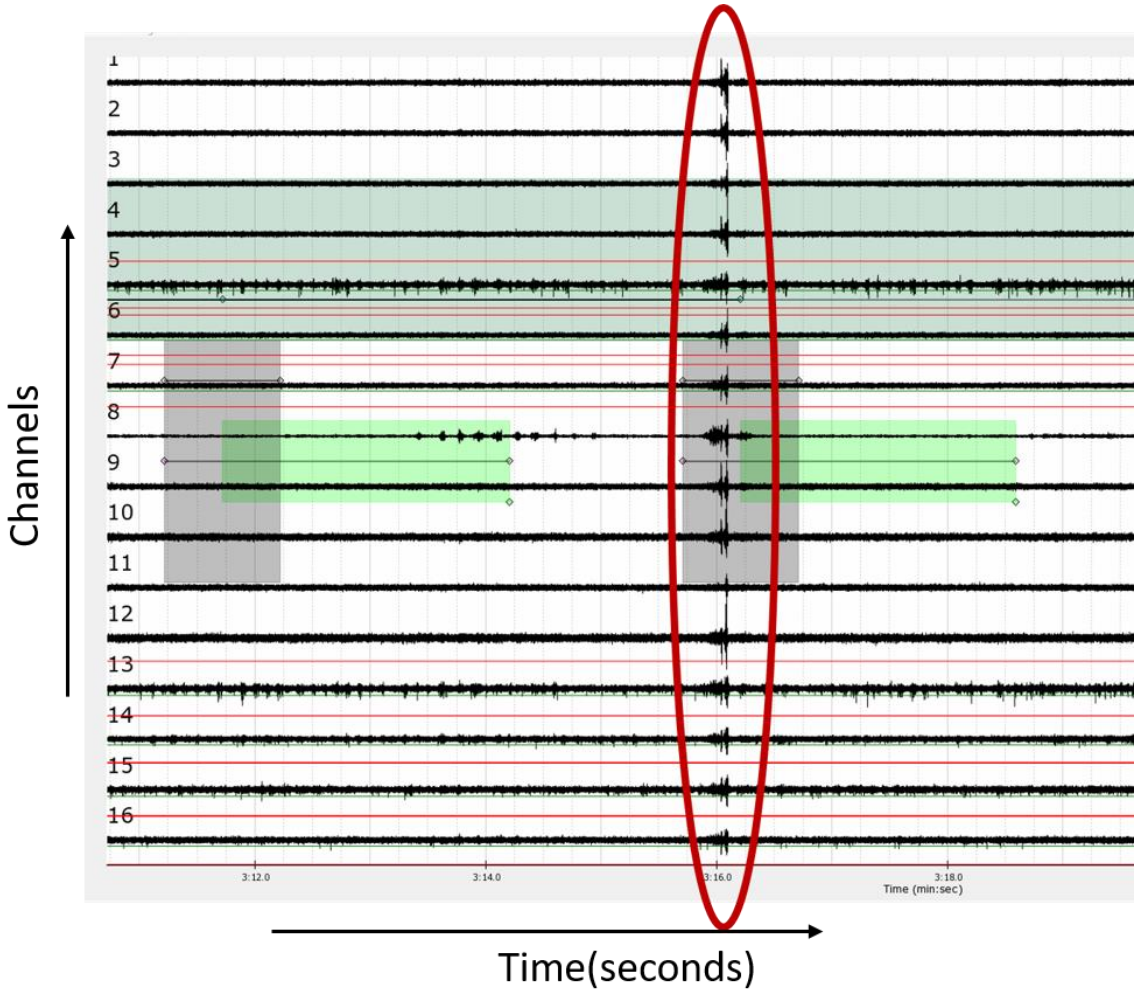

Figure 2.7 Contaminated trial in a session. The trial on the left is an uncontaminated trial. In the second trial, there is a presence of common noise through all the channels (red circled) and termed as contaminated trial.

2.1.3 ROC Plotting

Receiver-operating characteristics can be deployed to examine the performance of a classifier. The following example illustrates the principle of ROC analysis. Moving the criterion on the probability distribution, we get the False positive rate and True positive rate at every level (Figure 2.8). These rates are plotted on the curve for every criterion value with True positive rate on the y-axis and False positive rate on the x-axis.

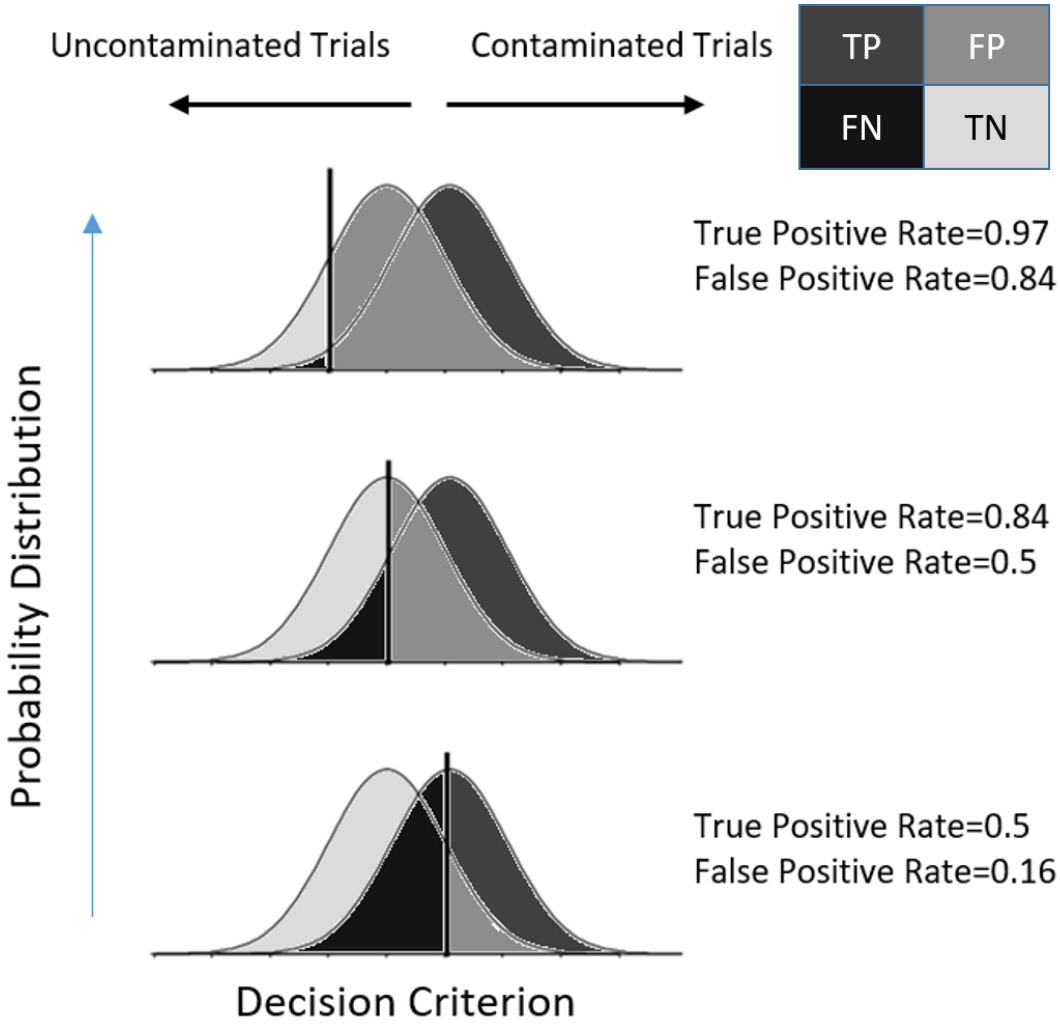

Figure 2.8 Effect of moving criterion on the probability distribution.

With increasing criterion level from left to right i.e. , from C1 to Cn, the false positive and true positive rate goes on decreasing as shown in Figure 2.9(A) and Figure 2.9(B). The rate of decrease for the false positive and true positive rate depends on the overlapping between the two distributions. Combining the amplitude information across multiple electrodes it is possible to obtain a sharpened distribution of potential artefacts and spike events, which will have minimum distribution overlap (Gockel et al., 2010).

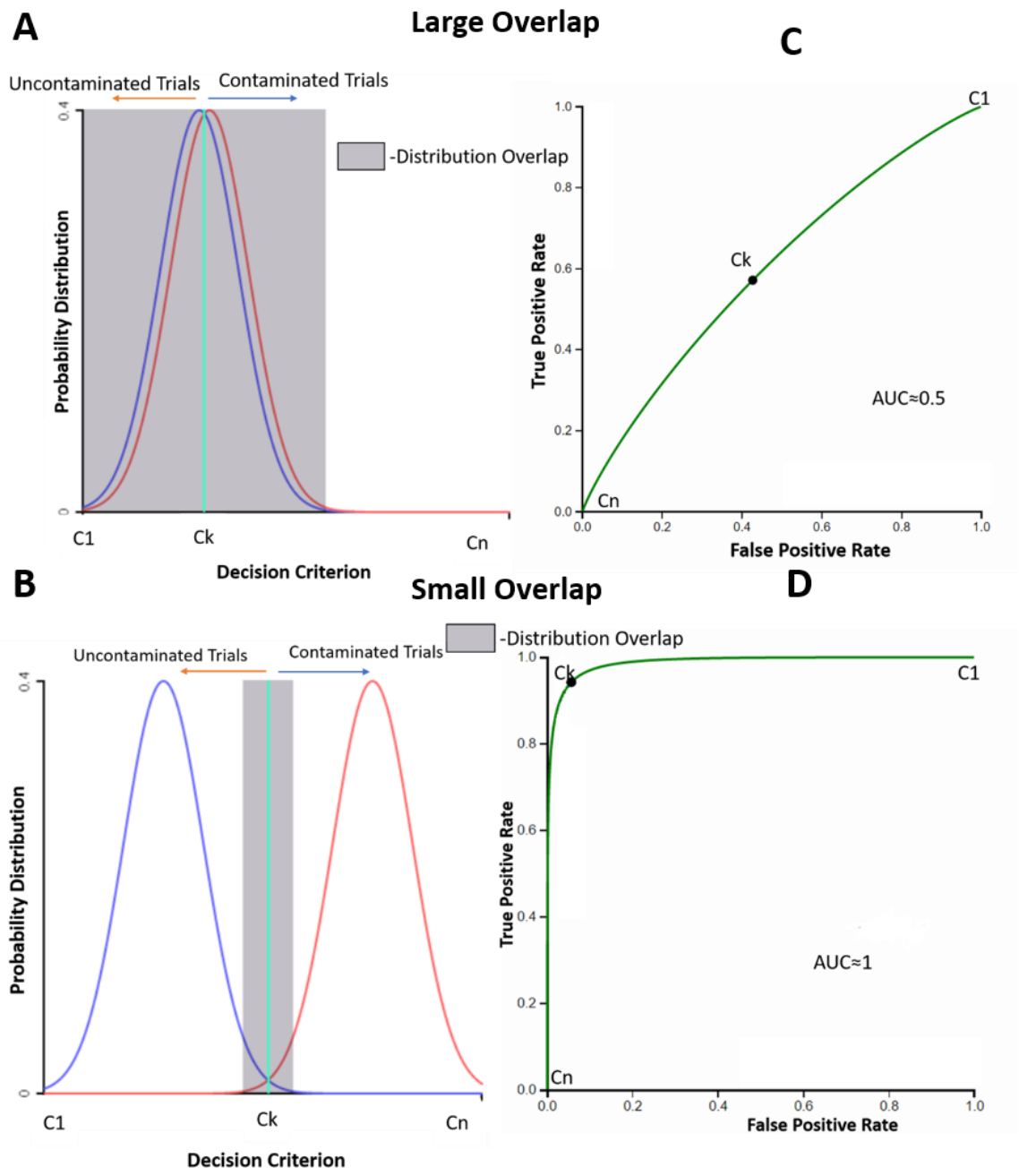

Figure 2.9 Probability Distribution and ROC curve. The decision criteria moves from left to right in the distribution(left), giving out false positive rate and true positive rate which is plotted on the ROC curve(right) corresponding to the criterion level. The ROC curve varies with their distribution overlapping (gray).

2.3 ROC Comparison

To decide the optimal denosing algorithms between the two (IEC and AR), both their ROC's are compared with the area under the curve (AUC) . The accuracy of the classifier is measured by the area under the ROC curve (AUC) which is is calculated by trapezoidal rule. The area under the ROC curve (AUC) is a measure of how well the classifier can distinguish between two groups (common noise and normal). An area (AUC) of 1 represents a perfect test; an area of 0.5 represents an uninformative test. The classifier which derives the ROC curve with AUC=1 is considered an ideal classifier. Figure 2.5(B) shows that when there minimal distribution overlapping, the ROC curve has AUC ≈1. Indeed, this high probability distribution with minimal overlap permits the application of an ideal classifier for further processing. Previous work by Hanley and McNeil [Radiology 1982 143 29-36] suggests that even if the AUCs for both algorithms are similar, this does not necessarily mean that the curves are the same. Here, to decide whether the curves are different bivariate statistical analysis was performed. Standard error of the difference between the two areas was calculated followed by p-value (one-tailed). In this study, the AUC is used as a parameter to compare ROC and eventually the accuracy of different algorithms.

$$SE = \sqrt{\left(\frac{A(1-A) + (\mathrm{Nc}-1)(Q1-A^2) + (Nn-1)(Q2-A^2)}{Nc \times Nn}\right)} \tag{2.3}$$

$$\mathrm{Q1} = \frac{A}{(2-A)} \tag{2.4}$$

$$Q2 = \frac{A^2}{(1 + A)} \tag{2.5}$$

$$\text{SE (A1-A2)} = \sqrt{SE^2(\text{A1}) + SE^2(\text{A2})} \tag{2.6}$$

$$\text{p} - \text{value} = \frac{A1 - A2}{SE(A1 - A2)} \tag{2.7}$$

Nc: Number of contaminated trials.

Nn: Number of uncontaminated trials.

A: Area under the ROC curve.

SE: Standard Error.

2.4 Kneepoint

In a ROC curve, the true positive rate is plotted as a function of the false positive rate for different criteria values of a parameter. For the specific recordings analyzed here, most ROC curve revealed a knee point beyond which the false positive rate was no longer affected by the criterion choice. Thus, the knee point reveals the criterion for which the false positive rate is close to minimal and the true positive rate close to maximal.

The knee point on the ROC curve was determined by walking through each pair of consecutive points of the ROC curve, fitting two lines, one to the left and other to the right of each pair of points. The point which minimized the sum of errors for the two fits was judged as the knee point. Figure 2.9 shows an example kneepoint (Ck) where the false positive was minimal and at the same time true positive area was maximal.

In this study, there are three classifiers which are used independently as well as in combinations. This ROC analysis evaluated the effectiveness of these algorithms in discarding common noise. These ROC curves were then compared with each other with AUC as the parameter.

2.5 Spike Rate

ROC compared the accuracy of common noise reduction from all the above mentioned algorithms. The algorithm with highest AUC was considered as the optimal solution in denoising the electrophysiological data. The noise reduced spikes were obtained from a time window from all the electrodes. The spike rate, i.e. the number of spikes in a time window, was calculated for every trial and averaged across the trials with same sound intensity level for every electrode

$$Spike\ rate = \frac{Number\ of\ Spikes}{Time\ duration} \tag{2.8}$$

To illustrate the neuronal firing patterns, Spike rate was normalized through z-score, which was calculated by subtracting the spike rate across same sound intensity levels from the overall firing rate, and then divided by the standard deviation of the overall firing rate.

$$z - score = \frac{TMR\ Spike\ rate - Overall\ spike\ rate}{Standard\ deviaton(Overall\ spike\ rate)} \tag{2.9}$$

CHAPTER 3

METHODS

3.1 Experiment

Animals (3 Normal Hearing and 1 Hearing impaired) were trained and tested on a target detection task using a Go/NoGo paradigm, as described previously (Buran et al., 2014). The animals were freely placed in the cage with recording electrodes implanted in the left auditory cortex(Figure 3.1) with ground contralaterally placed and voltage traces were recorded while animals passively listen to the stimuli(see stimuli section) delivered through an overhead speaker (Buran, von Trapp, & Sanes, 2014) (Figure 3.2). Neural recordings were obtained using a multichannel acquisition system at a sampling frequency of 24.4 kHz with a 16-channel (15-electrodes and 1-ground electrodes) wireless headstage and receiver was used in conjunction with a preamplifier and analog-to-digital converter (Figure 3.3). The electromagnetic setup induces noise (non-neural activity) in low-amplitude electrophysiological signal along with the neural activity (Gagnon-Turcotte et al., 2015).

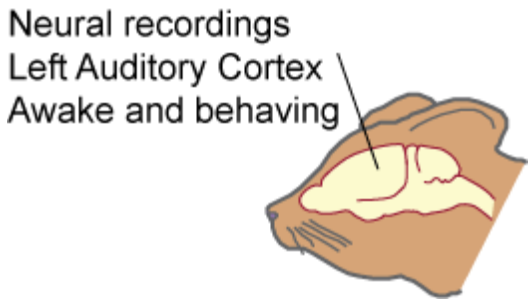

Figure 3.1 Location of electrode placement.

Some implanted electrodes in the auditory cortex do not transmit any signal due to broken contact during the surgery or device malfunctioning. These electrodes are termed as “broken electrodes”. These electrodes are rejected in the analysis.

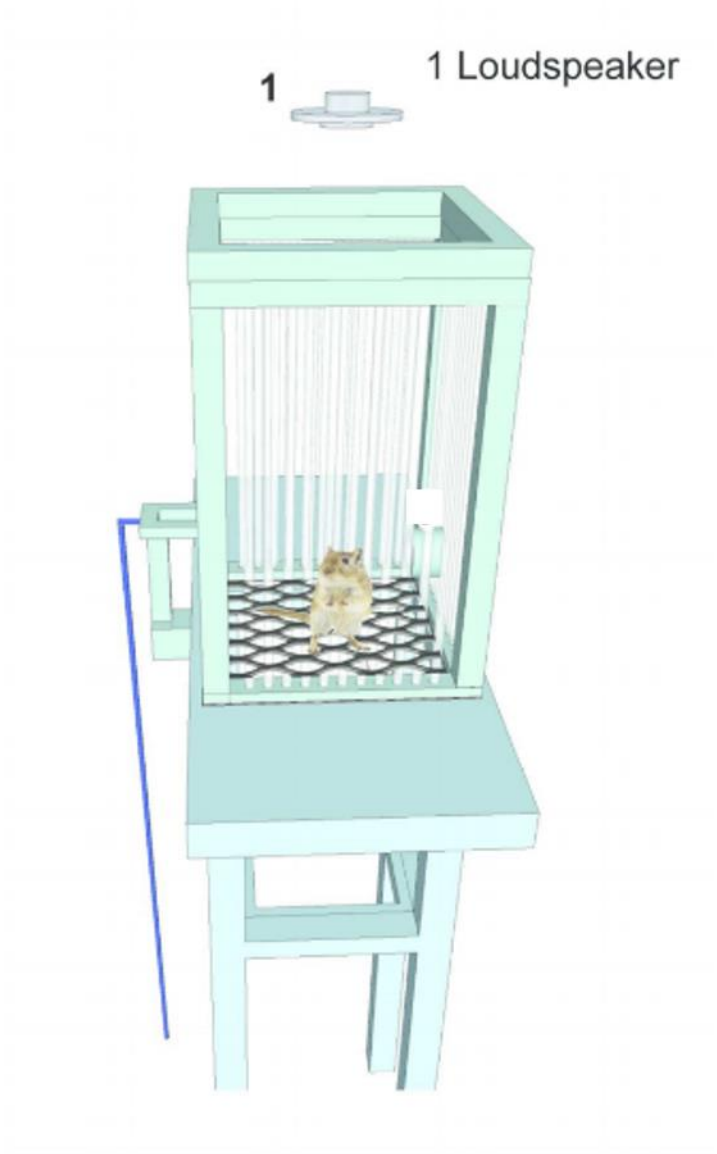

Figure 3.2 Experimental Setup.

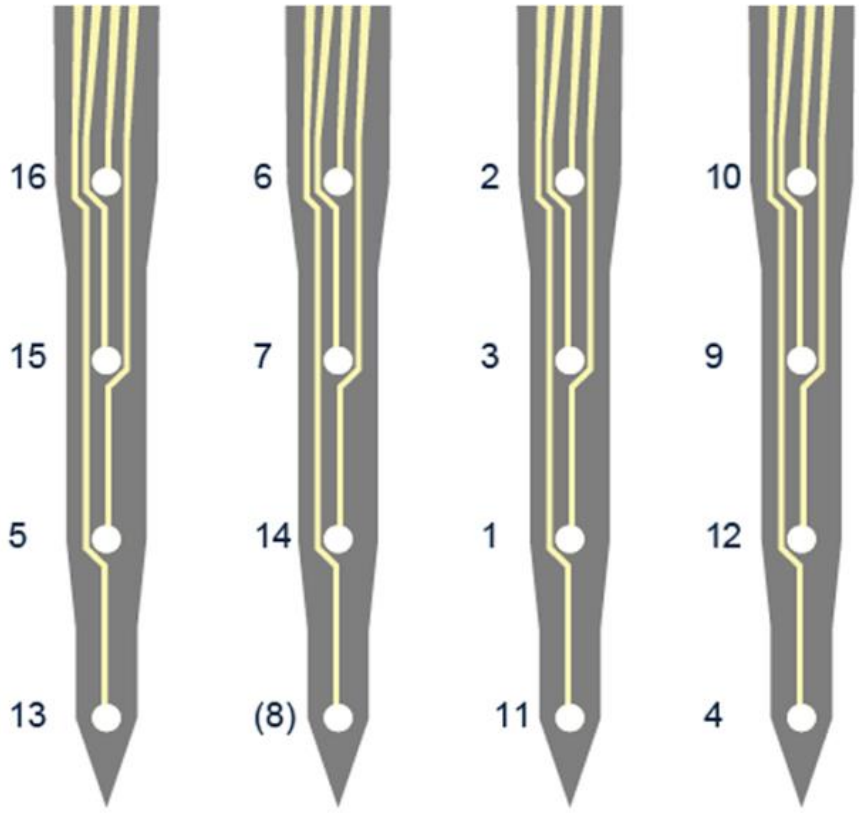

Figure 3.3 Array of micro-electrodes.

3.1.1 Stimuli

In the study, each target on a Go trial consisted of a 1 -kHz tone of 1 second duration. On NoGo trials, no stimulus was presented. The target tone was presented with noise envelopes either unmodulated or modulated with a 10-Hz rectangular waveform.

These maskers had an additional flanker component, centered at 3 kHz which were constructed with identical frequency and phase (Ihlefeld et al., 2016). These Stimuli were randomly presented in six different Target-to-masker ratio (TMR) dB SPL (decibel, Sound pressure level) to explore the spike rate at different intensities. TMR is expressed as the

difference in level between the target and each masker. Thus, if the target level is 50 dB SPL and each masker is also 50 dB SPL, the TMR is 0 dB.

Specifically, two types of stimuli were used in this study:

1) Unmodulated on-target noise (M2).

2) Modulated on-target noise (M4).

In this study these two types of stimuli are termed as M2 for Unmodulated on-target noise and M4 for Modulated on-target noise.

These stimuli type varied randomly from session to session, and stayed fixed throughout each session for both NH and HI animals. 52 recordings were collected out of which 42 were of NH (M2=21 and M4=21) and rest of 10 were of HI (M2=5 and M4=5).

3.2 Pre-Processing

52 datasets were recorded, each consisting of one session of voltage trace recordings from implanted microelectrode arrays in gerbil's auditory cortex. Sessions varied in the number of trials. All processing and analysis were carried out using custom developed scripts in MATLAB. Using 4^{th} order Butterworth filters with zero-phase, each dataset was initially bandpass filtered between 300Hz - 6 kHz using the command 'filtfilt' in MATLAB. Using visual inspection, each trial in all of the recorded datasets was then classified as either uncontaminated or contaminated by non-neural noise. This classification serves as benchmark for all subsequent analysis. Specifically, subjective assessment of common noise was performed by an experienced researcher in electrophysiology to help determine the contaminated trials. The researcher marked all the trials as "contaminated trials" which appeared to have common noise due to characteristic temporal patterns commonly

associated with animal movement which would be seen in all the channels or whose signal amplitude was unusually high compared to median amplitude of the recordings. The user indirectly determines the uncontaminated trials (true condition positive) and contaminated trials (true condition negative). Each of the 52 datasets had common noise in at least one trial (Duda et al., 2012). Following this pre-processing, three different classifiers were applied for detecting the common noise present across multiple electrodes and thus improving spike detection, as described below.

3.3 Amplitude Threshold

The amplitude threshold method detects events as follows. When the voltage exceeds a threshold value, the 2.1 ms (milliseconds) of the voltage trace surrounding threshold are classified as "event" (Quiroga, 2007). As a result, each event's waveform segment has 51 sample points, 27 sample points preceding local minima and 24 sample points following the local minima (Figure 3.4). In intra-cellular recording, the phenomenon of neuron-burst leads to multiple neuronal firing in small amount of time (<3ms), which leads to multiple spike detection within one event. In order to avoid one event triggering multiple threshold crossings, there is a short period of time, which turns off detection (1ms) after every threshold crossing, the so-called "censoring" (Hill, Mehta, & Kleinfeld, 2011).

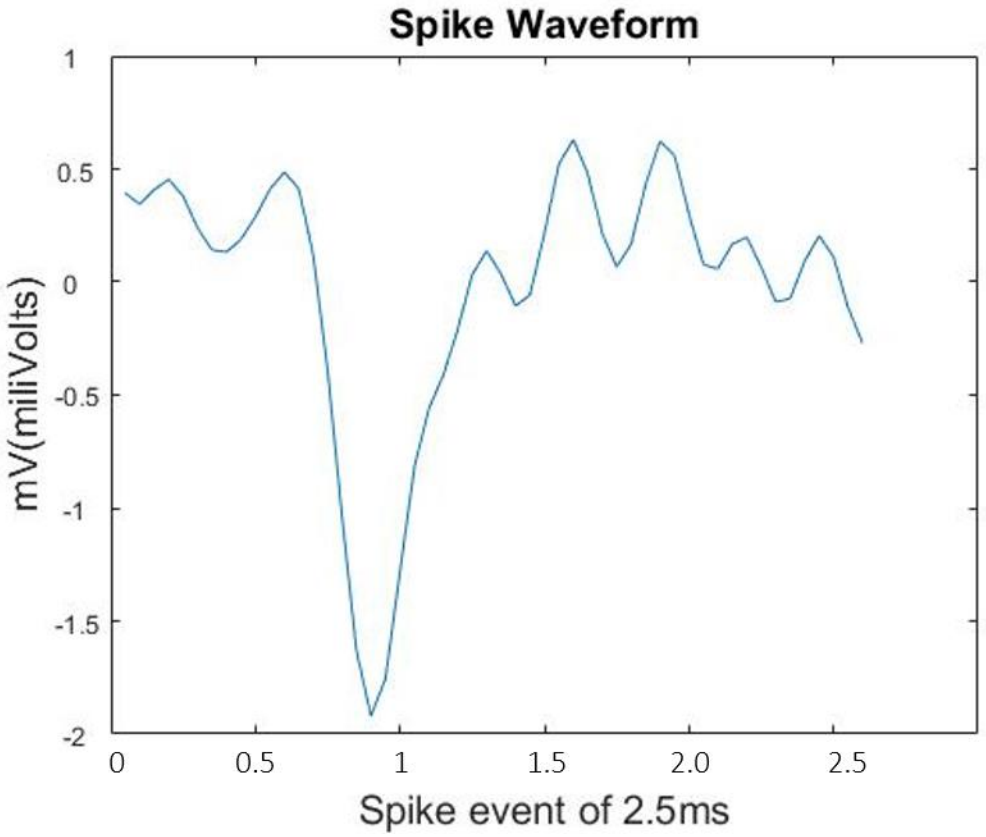

Figure 3.4 Detected spike waveform of duration 2.1 ms and 51 sample points.

If the value of the threshold is too small, noisy activity will lead to false positive events, if it is too large, low-amplitude spikes will be missed. Thus, there is a need to determine the range of amplitude thresholds that lead to the low false positive rate and high percent true positive. In addition, artefacts from animal movements and interference due to wireless headstage cause addition of large-amplitude signal that typically exceed the maximal amplitude of a neural spike event (Gagnon-Turcotte et al., 2015). One solution proposed in the literature is to use a value based on the standard deviation of the signal of respective channel.

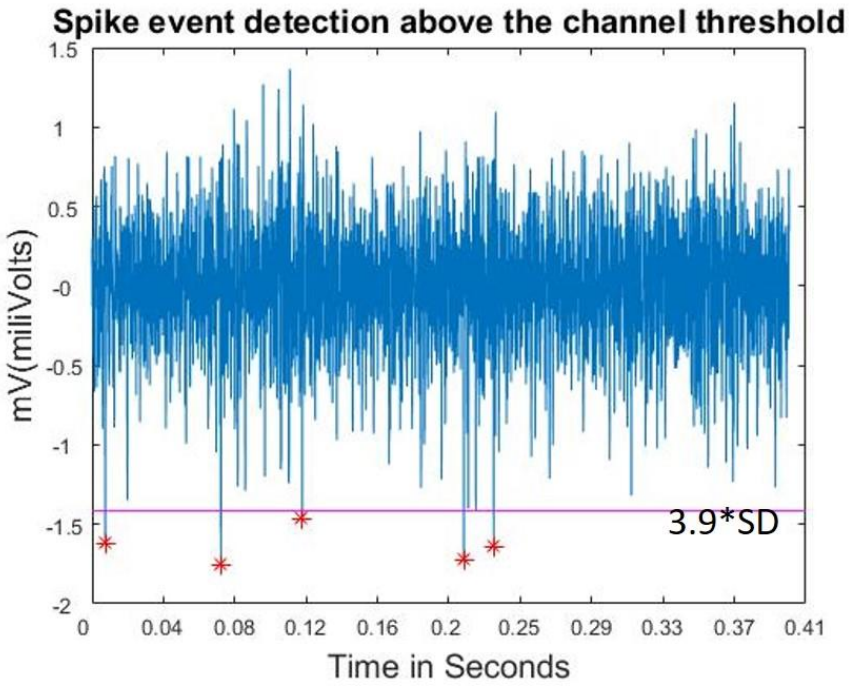

Figure 3.5 Spike event detection above 3.9 * SD (Standard Deviation) of the respective channel.

To determine the optimal value for amplitude threshold, the events were classified as a spike if they fell within a range of amplitudes between 3.9 and 7 times the SD of their respective channel (Figure 3.5). 7 times SD is the knee point of the ROC (Receiver Operative Characteristics) for Amplitude Rejection algorithm (discussed further). For each channel, all the detected spike events are saved as waveforms.

3.4 Amplitude Rejection

In Amplitude Rejection (AR), the spike signal which exceeds a certain threshold would be rejected from being considered as spikes. The basic idea of Amplitude rejection (AR) is to estimate the common noise floor for each channel and eventually throughout the whole dataset. Signal detection theory gives an estimate of the amplitude threshold for discarding the spikes events.

In AR, at every decrementing steps of 1 standard deviation starting from the mean to the minimum of the trial data of all electrodes (Figure 3.6), the trial is counted as predicted condition positive and if this particular trial is one of the true condition positive, then it is a true positive. So at every 1 standard deviation step, the true positive rate and false positive rate is calculated i.e. by moving the decision criterion from mean to minimun. Using these rates the ROC is plotted. Such ROC curve is plotted for every channel, as every channel has different noise floor.

Using the knee point of the ROC, a criterion threshold in units of standard deviation of the median recorded voltage is then estimated to classify trials contaminated by common noise. With decreasing threshold, the false positive rate and true positive rate both increase (Figures A1 and A2).

The standard deviation at the knee point of this curve is considered here as the threshold for spike event rejection of that channel. The detected spikes events are discarded if the spike exceeds this threshold of respective channels.

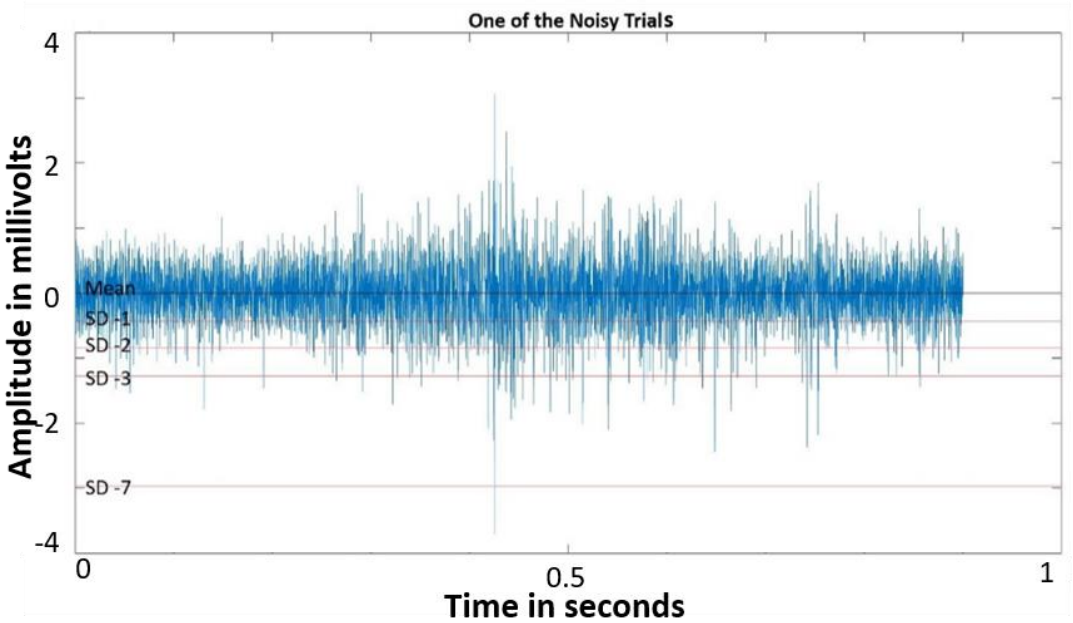

Figure 3.6 Contaminated trial and decrementing SD. The above signal is 1second data from a contaminated trial of one of the electrode. The black line is the mean, and the red lines are the decrementing standard deviation till it reaches the minimum of the signal. For every decrement in the standard deviation as the threshold, it is checked with the contaminated trial data (true condition) to derive the detection rate. For example; at SD= -1, which is near the common noise floor, every trial would be detected as true positive and false positive thus the detection rate would be 1. Whereas at SD= -7 the trial would be true positive (in this case), since it exceeds the threshold and it is a contaminated trial.

3.5 Inter-Electrode Correlation

Common noise is generally present on all recording electrodes. Presence of common noise will trigger spike events simultaneously across all the electrodes. In the implementation of IEC algorithm, detected spike events are stored as waveforms in the matrix of respective channels. Each candidate spike identified on the test electrode is compared with the concurrent spike events which lie in 5 ms window of other electrodes. The correlation coefficient is then computed between the candidate spike waveform and the spikes on the rest of 15 electrodes in the 5 ms window. Upon exceeding the correlation coefficient above the predetermined threshold of 75%, the spike events on the respective electrodes were

marked and the electrodes are termed as “spike-correlated electrodes” (Paralikar et al., 2009) (Figures 3.7, 3.8 and 3.9).

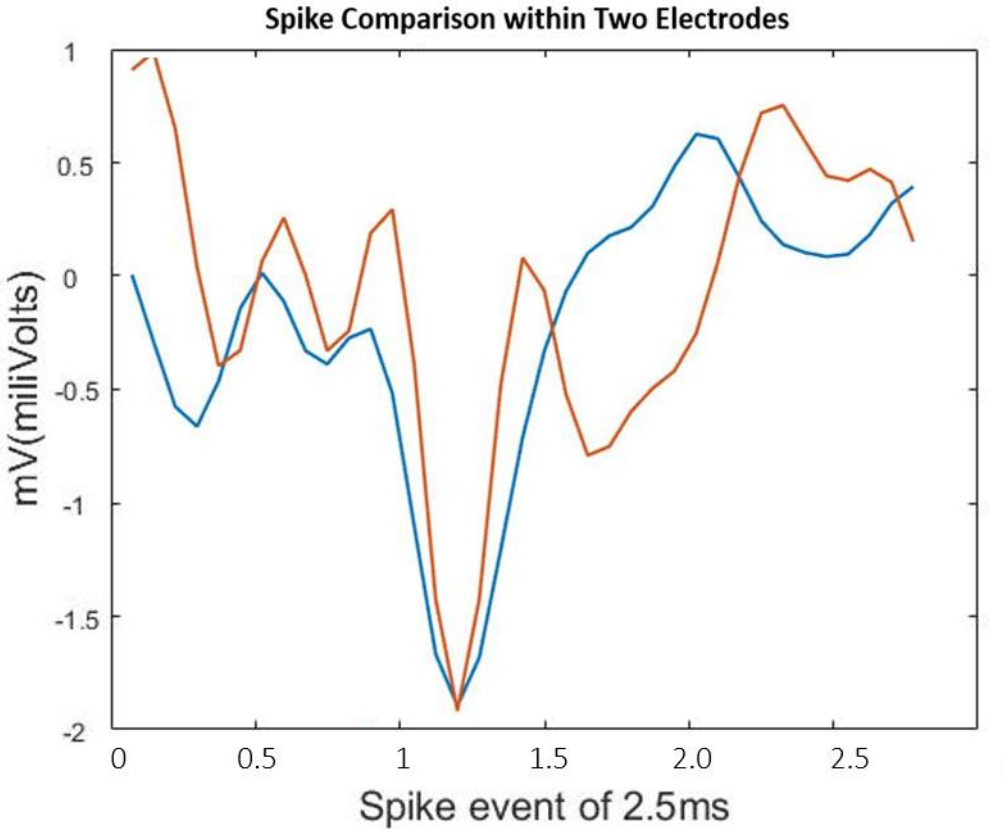

Figure 3.7 Waveform comparison between two spike events in different electrodes. The above figure shows the spike event waveform which occurs at the same time (or window of 5ms) in two electrodes. The correlation between these waveforms is computed, and these events are discarded if the correlation coefficient exceeds above the 75%, indicating the presence of common noise. This process is done on all channels.

The number of spike-correlated electrodes after spike correlation depends on the presence of common noise. Spike-correlated electrodes may vary from 2 to 16 electrodes, as two electrodes suggests a lower possibility of common noise as neurons nearing different electrodes location may respond simultaneously, whereas 16 electrodes clearly suggest the spike events as a common noise or non-neuronal activity. Multiple neurons may simultaneously respond to the acoustic stimulation also leading to concurrently activated electrodes. There is a need to decide a number of spike-correlated electrodes between 2

and 16. Signal detection theory was used to decide number as the threshold. If the concurrent spike events are common in more than this threshold, then the spike event is rejected as common noise.

The number of spike-correlated electrodes after IEC analysis in a trial is proportional to the presence of common noise, the trials with more than two spike-correlated electrodes (further incremented, i.e., from 2 to 16 electodes) is counted as predicted condition positive and if these trials are the same trial as the true condition positive, then it is a true positive. Further its true positive rate and false positive rate is determined for incrementing spike-correlated electrodes. Similarly, true positive rate and the false positive rate is determined for all spike-correlated electrodes by moving the decision criterion from lower number of electrodes to higher number. To analyze the performance of this algorithm and to get an discrimination threhold, ROC curve is plotted using true positive and false positive rates for all the electrodes. On comparing the true condition and the predicted condition for the incrementing (i.e., from 2 to 16 electrodes) spike-correlated electrodes, the false positive rate decreses at a higher rate than the true positive rate as shown in Figure 2.12. The point (electrode number) where the true positive rate is comparatively high and false positive rate is low is considered as a kneepoint.

The knee point is calculated with the same method explained previously. The channel number at the knee point is considered here as the minimum number of spike-correlated electrodes required for rejecting the event as a common noise. The similar spikes (correlation coefficient >0.75) occurring at the same time in multiple electrodes is discarded if they are present in more than number of electrodes decided by the knee point analysis derived from the ROC curve.

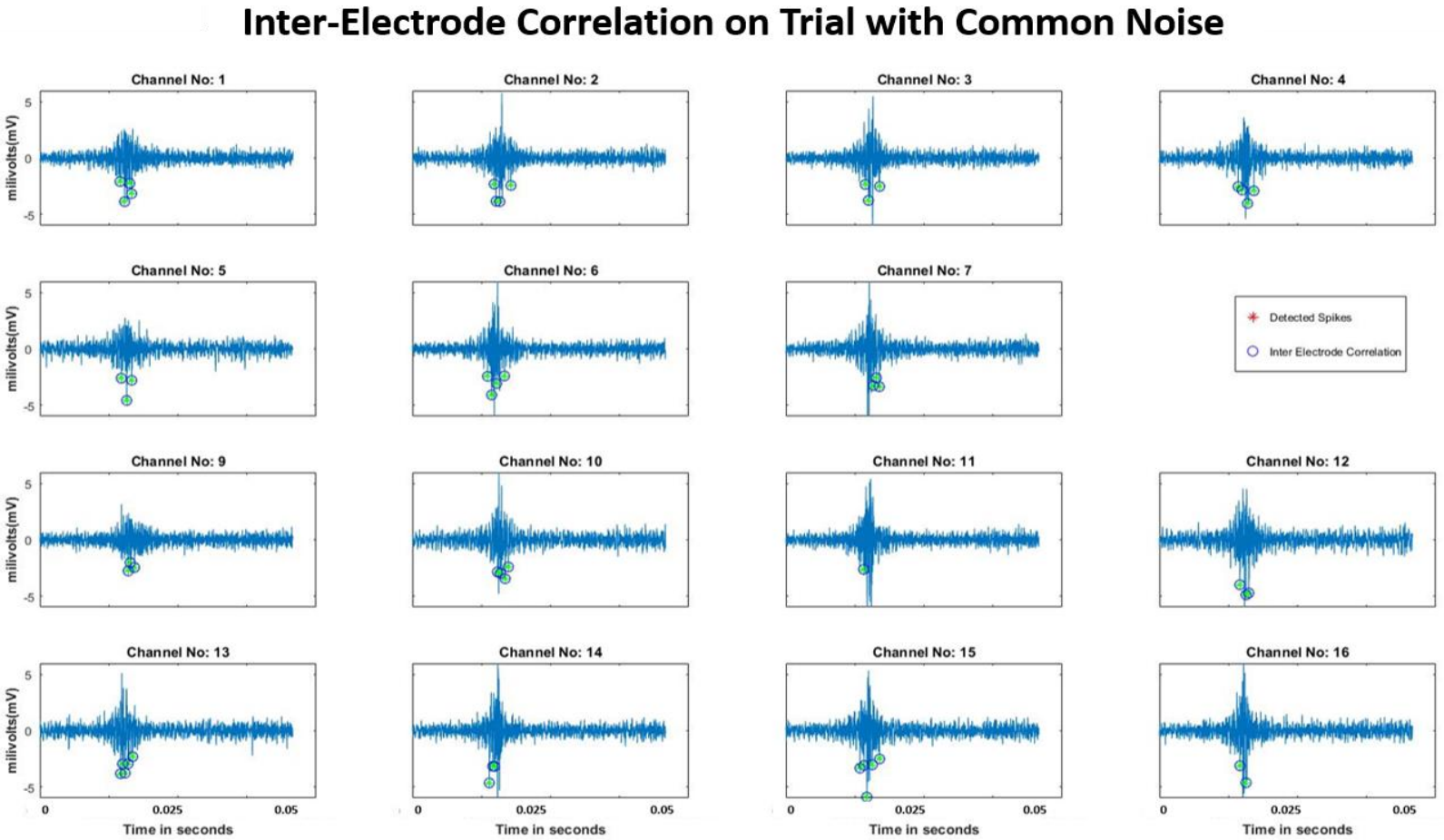

Figure 3.8 Inter-electrode correlation on a snippet of a signal between all the channels in a contaminated trial. The above figure shows the implementation of IEC algorithm on a contaminated trial. After the spike detection (*), the candidate spike is compared with the spike events concurrently in the window of 5ms in the rest of the electrodes. The spike events are discarded if the compared spike waveforms exceed the correlation coefficient of 0.75. Discarded events are marked as *. In the above trial, the same spike event across all the electrodes exceeds the coefficient at the same time, which clearly affirms the presence of common noise.

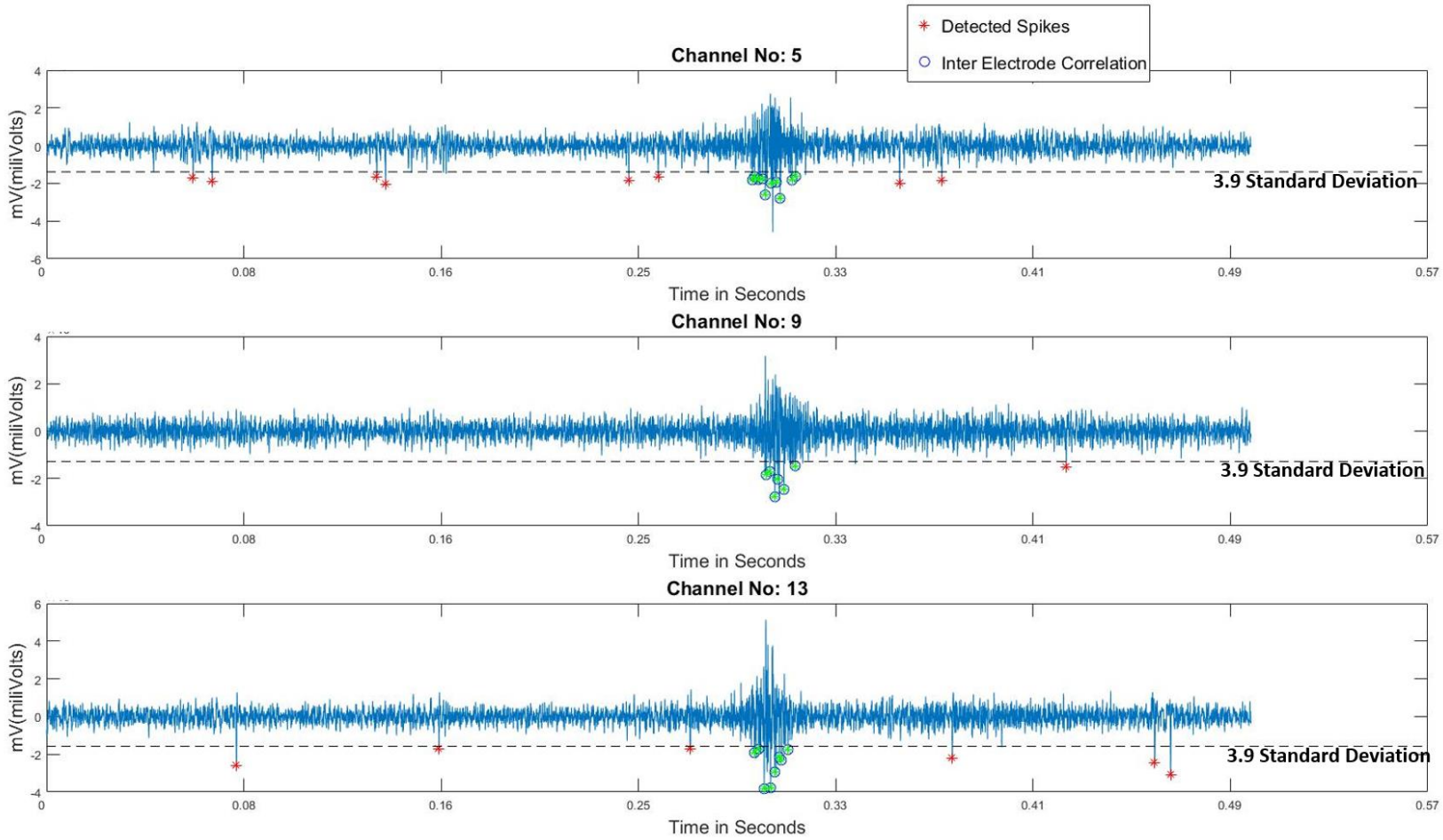

Figure 3.9 Inter-electrode correlation on a snippet of a signal between 3 channels in a contaminated trial. After the spike detection (*) at 3.9 standard deviation of the respective channel, the candidate spike is compared with the spike events concurrently in the window of 5ms in the rest of the electrodes. The spike events are discarded if the compared spike waveforms exceed the correlation coefficient of 0.75. Discarded events are marked as *. In the above trial, the same spike event across all the electrodes exceeds the coefficient at the same time, which clearly affirms the presence of common noise.

3.6 Virtual Reference

In Virtual reference (VR), the grand mean of the signal from all the electrodes is subtracted from the electrode of interest (Paralikar et al., 2009). The use of VR reduces common noise floor in all the electrodes, which reduces the number of false alarm rate of spike detection. This technique helps lower the overall noise floor of the recorded signal, but it may also result in undesired cancellation of correlated neural activity. To examine the potential use of VR for the current data set, both the AR and IEC algorithms were implemented in two parts, 1) with VR 2) without VR and then compared. These two algorithms are implemented independently and will have two independent results but to check their dependency, the IEC is implemented after AR and their results are compared (Figure 3.10).

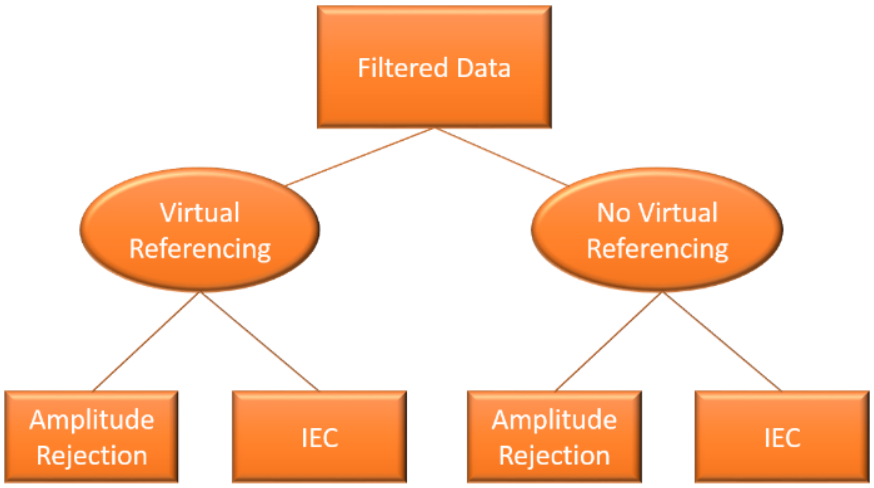

Figure 3.10 Flow of analysis for further comparison.

3.7 Receiver Operating Characteristics

In this study, the ROC analysis evaluates the effectiveness of Amplitude Rejection (AR) and Inter-electrode correlation (IEC) algorithms in discarding common noise which are detected as spikes. It also validates the use of Virtual referencing for common noise reduction through the dataset.

The ROC curves plotted for the algorithms are compared with each other with area under the curve as the parameter (discussed in Background section). The knee point of these curve is considered as the decision threshold for the respective algorithm. Using the algorithm which has the maximum AUC and the kneepoint as its threshold, the spike rate is derived.

3.8 Spike Rate and its Analysis

Using the best suitable algorithm the noise reduced spikes are obtained from 1 second time window of tone presence from all the electrodes. Spike rate is calculated (as mentioned in Background) for every trial and averaged across the trials with same TMR for every electrode (Figure 3.11). Broken electrodes are rejected for further analysis as they show no spike patterns.

To illustrate the neuronal firing patterns, spike rate is normalized to z-score for different TMR. z-score is calculated across all the unbroken electrodes for every TMR in a session. Similarly, z-score is averaged across all the sessions from a similar group of datasets. The group average of the z-score is compared within two group of animals.

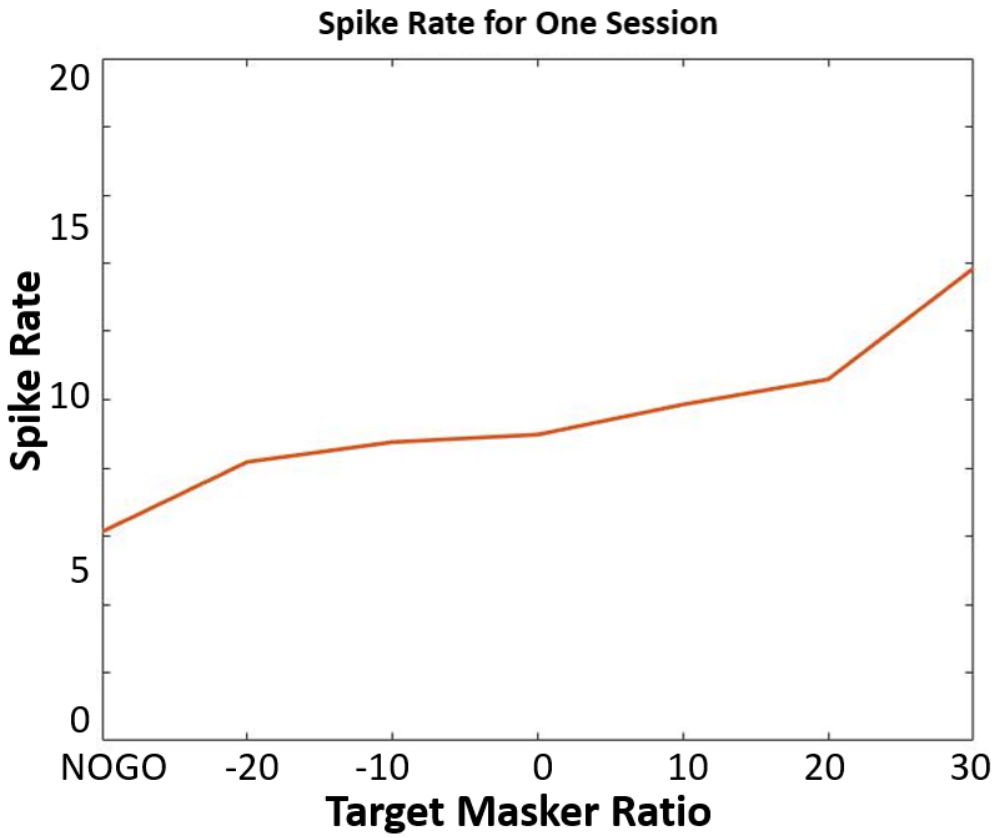

Figure 3.11 Spike Rate averaged over the trials with same TMR for one session.

To find out the effect of MMR between NH and HI animals, a comparison is carried out where the normalized spike rate data were analyzed with repeated measures analysis of variance (rANOVA). In this study, repeated measure of ANOVA (rANOVA) is used to study the interaction and correlation of spike rate between Modulated on-target noise and unmodulated on-target noise within Normal hearing and Hearing Impaired animals.

At normalized spike rate plots, TMR thresholds were extracted at z-score=1 for average across each animal for both the maskers (3 NH animal and 1 HI animal). For HI animal only three sessions are considered in rANOVA analysis (sessions which had the maximum above z-score=0.5). The rANOVA scripted in MATLAB 2016 gives a p-value (one-tailed), if $p<0.05$ then we reject the null hypothesis (Null Hypothesis: The spike rate between the groups are same).

CHAPTER 4

RESULTS

4.1 Denoising Algorithms Performance

To assess which noise rejection method results in optimal performance, the AR, VR and IEC algorithms were implemented in Matlab and tested in different combinations. Table 4.1 lists all tested variations. For each combination of classifiers, ROC curve were computed for each data set and subsequently average across all data sets.

Table 4.1 List of Variation of Algorithm in Order to Find Out Best Combination of Algorithm in order to get Optimal Performance in Noise Rejection

	List of Algorithms	
1	AR_{VR}	Amplitude rejection algorithm with Virtual Referencing
2	AR_{NoVR}	Amplitude rejection algorithm without Virtual Referencing
3	IEC_{VR}	Inter-Electrode correlation algorithm without Virtual Referencing
4	IEC_{NoVR}	Inter-Electrode correlation algorithm without Virtual Referencing
5	AR_{VR} + IEC_{VR}	Amplitude Rejection and Inter-Electrode correlation with Virtual Referencing
6	AR_{NoVR}+IEC_{NoVR}	Amplitude Rejection and Inter-Electrode correlation without Virtual Referencing

4.1.1 Amplitude Rejection

After the implementation of AR algorithm on all individual datasets the ROC curve derived for each session. An average ROC curve is derived across all the 52 datasets for both AR_{VR} and AR_{NoV}. To compare the effectiveness of VR in AR algorithm, ROC curves of AR_{VR} and AR_{NoVR} are compared, with AUC as the parameter (AUC for AR_{VR} = 0.753 and AUC for AR_{NoVR} = 0.748). The AUC is similar in both the cases ($p_{onetailed}$=0.483, level of

significance (α) =0.05). Figure 4.1 shows the ROC plot for AR_{VR} and AR_{NoVR} are almost similar and they both have 6 standard deviation as the kneepoint.

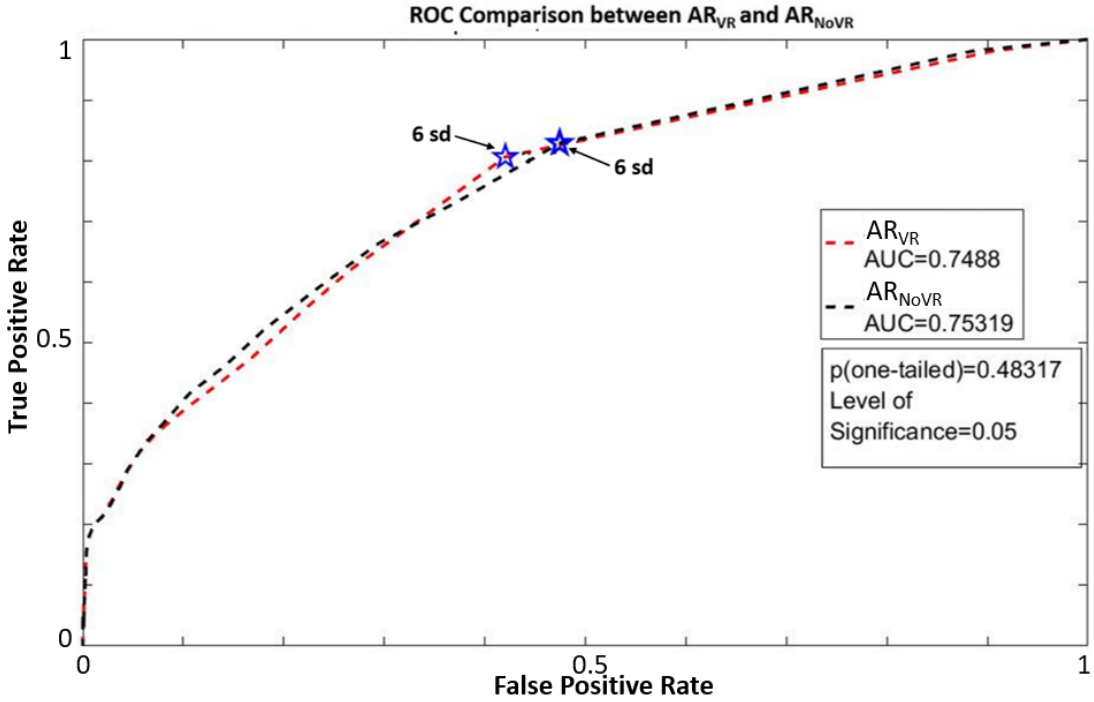

Figure 4.1 ROC comparison between AR_{NoVR} and $AR_{VR.}$ The ROC curve averaged over all the datasets, for AR algorithm with VR and without VR. The red dashed (--) is the ROC curve for AR_{VR} which is same as the ROC curve of AR_{NoVR} (Black dashed --) The AUC for the both the curve is same. The kneepoint for both the curve is the same as 6 standard deviation.

4.1.2 Inter Electrode Correlation

The ROC curve is derived for each session after implementation of each IEC algorithm with and without VR. The ROCs across all 52 datasets is averaged for both IEC_{VR} and IEC_{NoVR}, These two averaged ROCs are compared to check the potency of VR to reduce the common noise. The ROC curve of IEC_{VR} and IEC_{NoVR} were compared with AUC as the parameter (AUC for IEC_{VR} = 0.902 and AUC for IEC_{NoVR}=0.852). The AUC of IEC_{VR} is greater than IEC_{NoVR} ($p_{onetailed}$=0.271, level of significance (α) =0.05). The p-values suggests that there is no statistical significance in the two methods. In Figure 4.2, the ROC

curve for IEC_{VR} is much closer to the ideal ROC than IEC_{NoVR} and there is a significant change in the kneepoint. The IEC_{VR} (Kp=6) kneepoint is at lower channel number as compared to IEC_{NoVR} (Kp=9). The reduction in the kneepoint shows that the ability of VR in reduction of common noise which indicates lower probability distribution overlap.

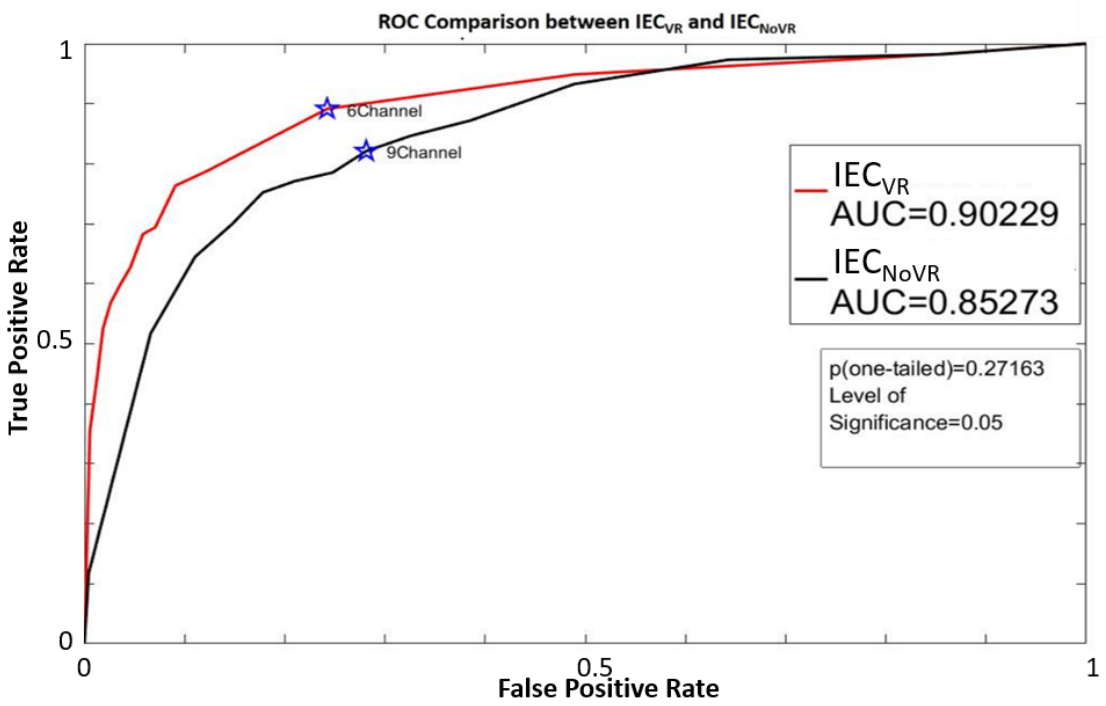

Figure 4.2 ROC comparison between IEC_{NoVR} and IEC_{VR}. The figure shows the ROC curve of IEC implementation with and without VR. The ROC curve for IEC_{VR} is red solid line (—) has more AUC when compared with ROC of IEC_{NoVR} black solid (—). The kneepoint of IEC_{VR} curve is 6-number of channels with common noise and for IEC_{NoVR} is 10 number of channels.

4.1.3 Combination of Amplitude Rejection and Inter Electrode Correlation

The filtered datasets with and without VR goes through spike detection and the AR algorithm is implemented. The kneepoint from the ROC curve of AR is considered as the amplitude threshold for rejecting the spike events. After discarding the spike events, IEC algorithm is implemented. ROC curve is derived for each sessions to decide a number of marked electrodes as the threshold for rejecting the spike event as the common noise. The

ROC curve is averaged over all the datasets. The averaged ROC curve for AR_{VR}+IEC_{VR} and AR_{NoVR} + IEC_{NoVR} are compared with AUC as the parameter (AUC for AR_{VR}+IEC_{VR}= 0.897 and AUC for AR_{NoVR} + IEC_{NoVR}= 0.844). The Figure 4.3 shows that the area is greater when the combination of algorithm is when implemented with VR ($p_{onetailed}$=0.263, level of significance (α) =0.05).The kneepoint lowers with the use of VR.

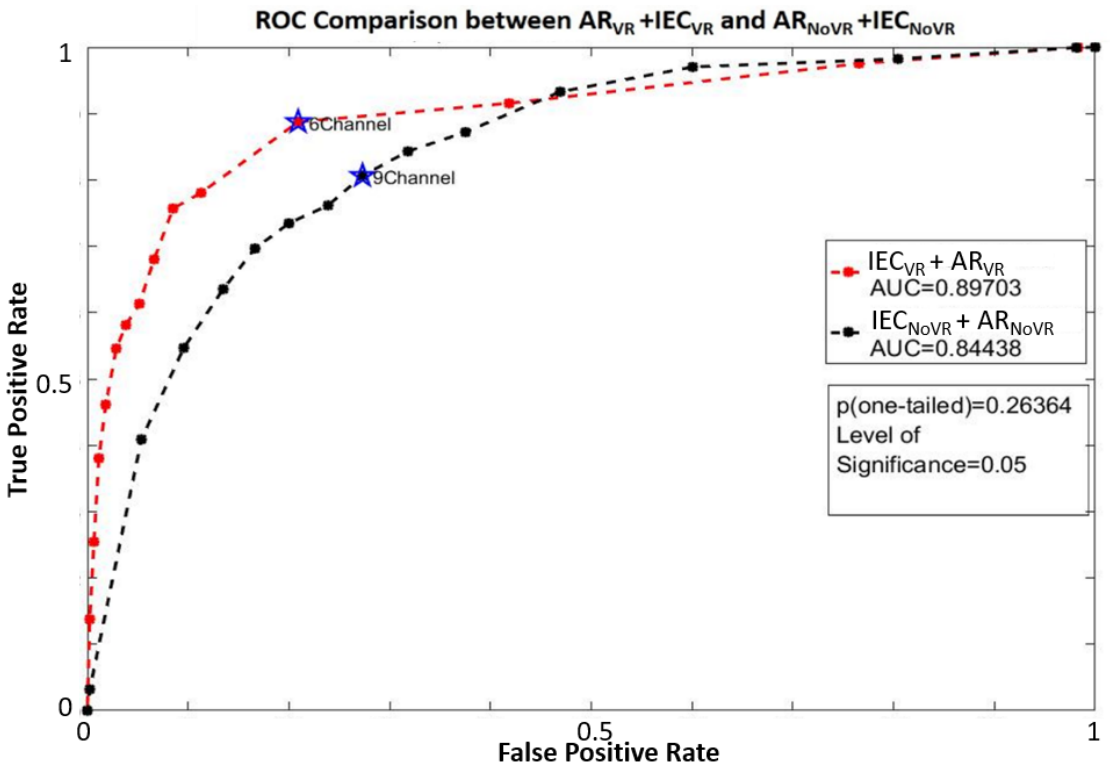

Figure 4.3 The ROC curves computed after implementing both AR and IEC with and without VR showed the difference in AUC. AR_{VR}+IEC_{VR} (-*-) has 6th channel as the kneepoint and AR_{NoVR}+IEC_{NoVR} (-*-) has 9th channel as the kneepoint.

4.1.4 Comparison between the algorithms

To compare the efficacy between two algorithms using VR in reducing the common noise, the ROC curve of AR and IEC were averaged over 52 datasets and compared. Comparing the two algorithms with AUC as the parameter, it shows a significant difference in the AUC between IEC_{VR} and AR_{VR} (AUC for IEC_{VR}=0.902 and AUC for AR_{VR}=0.748).There

is a statistical significance noted between these algorithms ($p_{onetailed}$=0.0454, level of significance (α) =0.05).

The similar comparison was done without VR on these two algorithms which show a comparatively difference in the AUC (AUC for IEC_{NoVR}=0.852 and AUC for AR_{NoVR}=0.753), but it is not statistically significant ($p_{onetailed}$=0.150, level of significance (α) =0.05) (Figures 4.4 and 4.5).

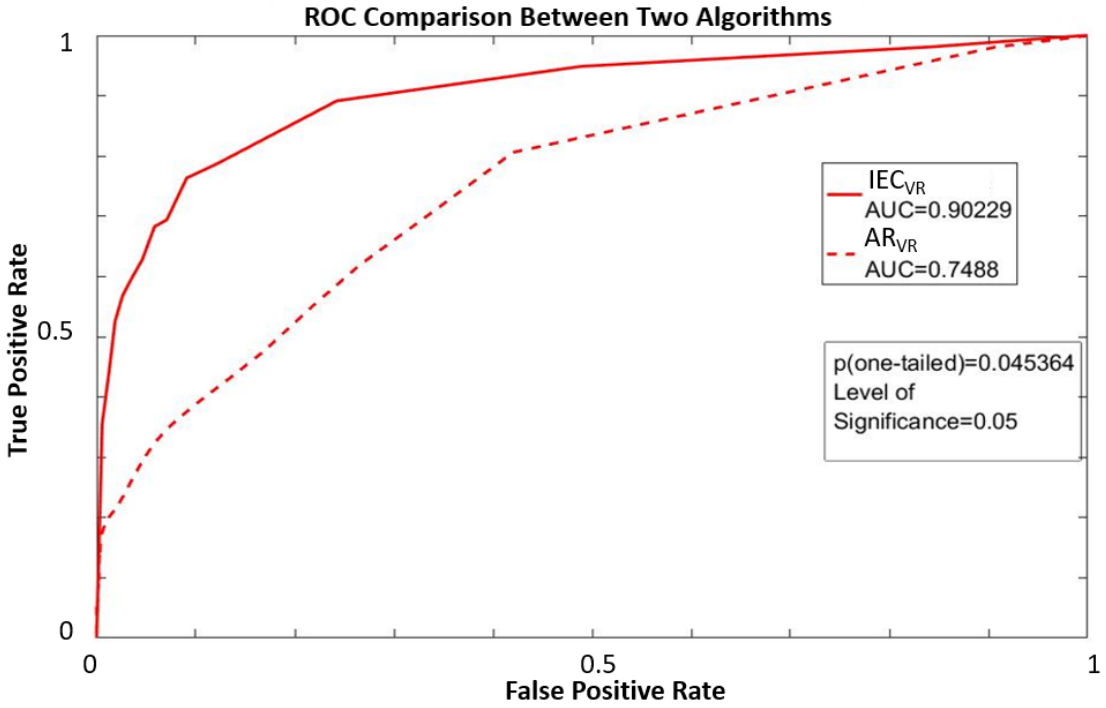

Figure 4.4 The ROC of AR and IEC are compared to test the result of both algorithms. There is a greater difference in the AUC of both. The p-value is 0.045 which is less than the level of significance.

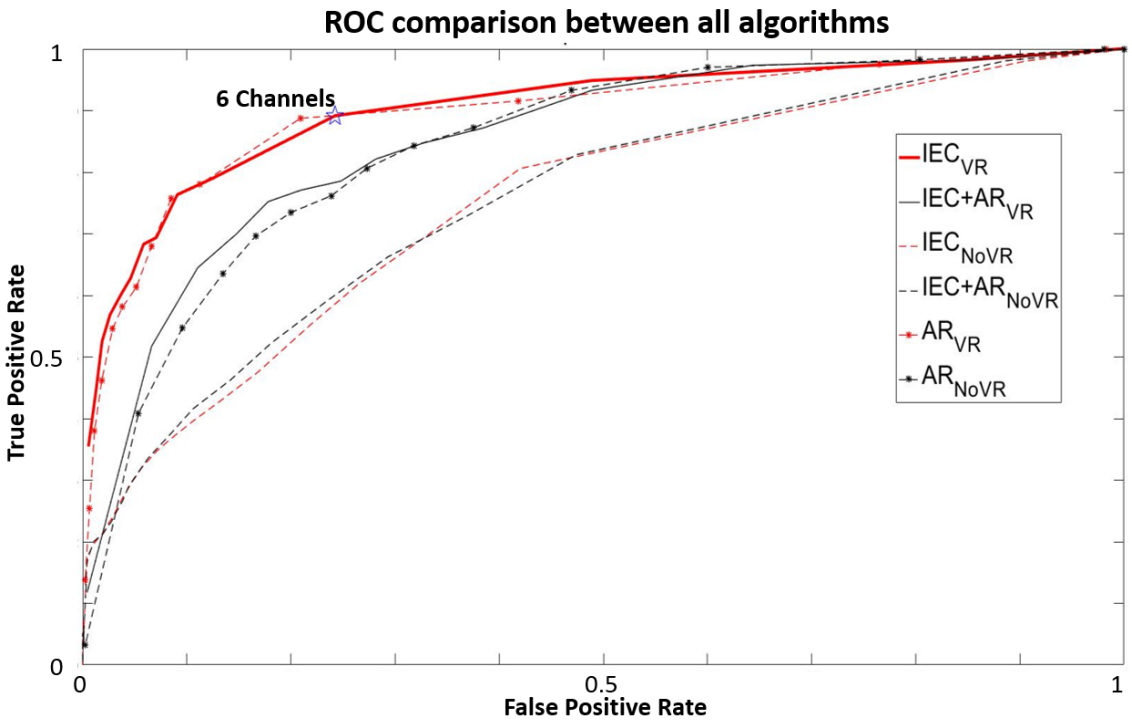

Figure 4.5 ROC comparison between all the combinations. Shows the ROC curve for different algorithms and their combination averaged over 100 dataset. The curves in red are when used with VR and black are when VR is not used. The solid line (--) is when IEC is used, dashed line when AR is used and (-*-) line when the combination of AR and IEC is used.

The performance of all the algorithms is ranked according to its AUC. Table 4.2 lists the AUC of all the algorithms, which shows that IEC_{VR} has the highest AUC and followed by AR_{VR} + IEC_{VR} which are almost similar in terms of the AUC value as well as ROC curve in Figure 4.5.

Table 4.2 List of Algorithm and their Respective Area under their ROC curve. The Algorithm with Higher AUC is considered as an Optimal Performance in Common Noise Rejection.

Algorithm Performance with AUC

	Algorithm	Area under the curve(AUC)
1	AR_{VR}	0.753
2	AR_{NoVR}	0.748
3	**IEC_{VR}**	**0.902**
4	IEC_{NoVR}	0.852
5	**AR_{VR} + IEC_{VR}**	**0.897**
6	AR_{NoVR} + IEC_{NoVR}	0.844

4.2 Neurometric Results

IEC and AR algorithms are compared with each other with and without the presence of VR, the algorithm with highest AUC derived from their ROC curve is used for spike rate calculation. The spike rate is calculated for every trial and averaged across the trials with same TMR for every electrode. Spike rate across one session is normalized through z-score for every electrode. These z-scores for unmodulated on-target noise (M2) and Modulated on-target noise (M4) are averaged across all the sessions for NH and HI animals.

4.2.1 Normal Hearing

The z-score (normalized spike rate) for both M2 and M4 shows an overall increase. The z-score for M2 stimuli increases slowly from -30 dB SPL to 0 dB SPL, but after that there is a steep increase after +10 dB SPL. The z-score for M4 stimuli show a constant increase in

the spike rate from -30 dB SPL to +30 dB SPL the rate of increase is low from -30 dB SPL till 0 dB SPL, but after that the z-score increases at much higher rate (Figure 4.6).

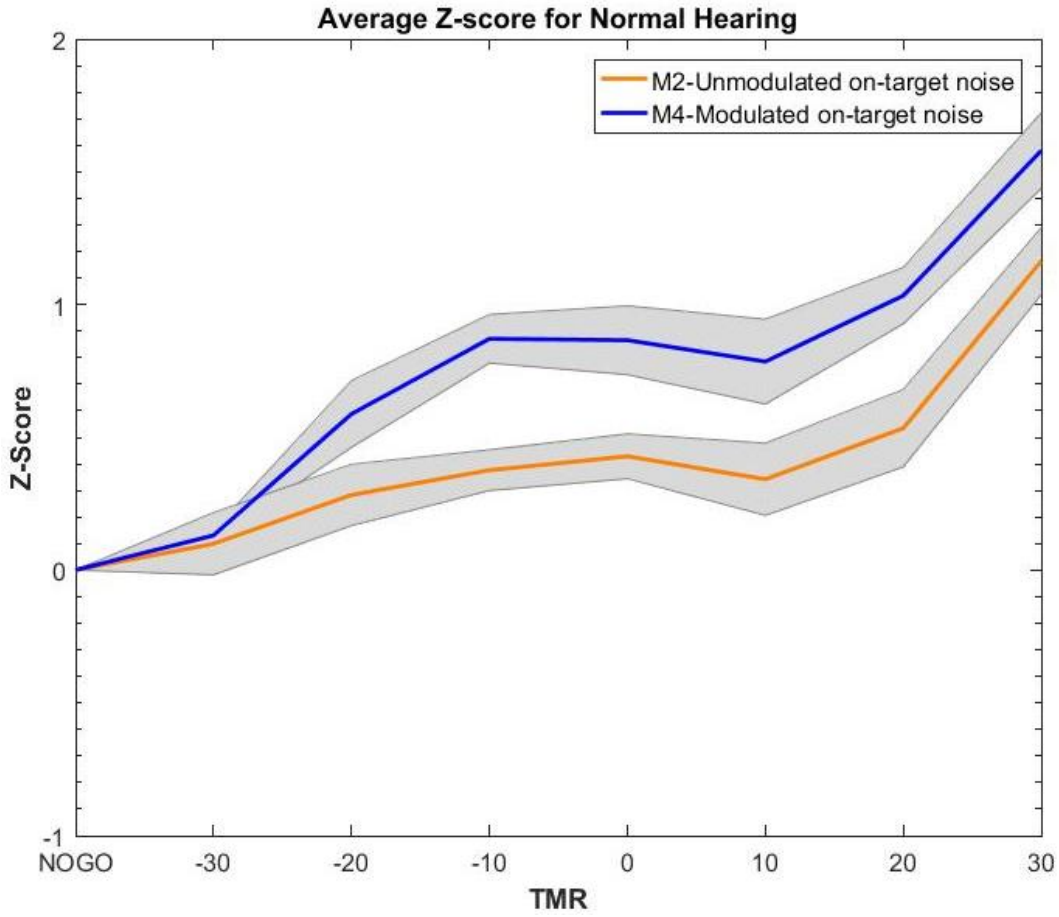

Figure 4.6 Normalized spike rate (z-score) for NH animals.

A threshold on the normalized spike rate of M2 and M4 were detected at z-score=0.5 for each NH animals averaged across sessions. The thresholds of each animal for both masker type is listed in Table 4.3 and their normalized spike rates is plotted in Appendix B. The results shows that thresholds for modulated masker are lower than unmodulated masker. To determine whether the modulated masker enhances the spike rate during target detection as compared to unmodulated masker, thresholds for both masker conditions were analyzed with rANOVA. The analysis found [$F_{(1, 4)}$ =0.49, p=0.55] that

the modulated masker when compared to unmodulated masker does not have statistical significance as p=0.55, rejecting the null hypothesis. The average MMR, defined here as the difference between the thresholds during total average of M4 and M2 in NH animals is 5.4 dB (M4 threshold= -18.2 dB, M2 threshold= -12.8 dB) shown in Figure 4.7.

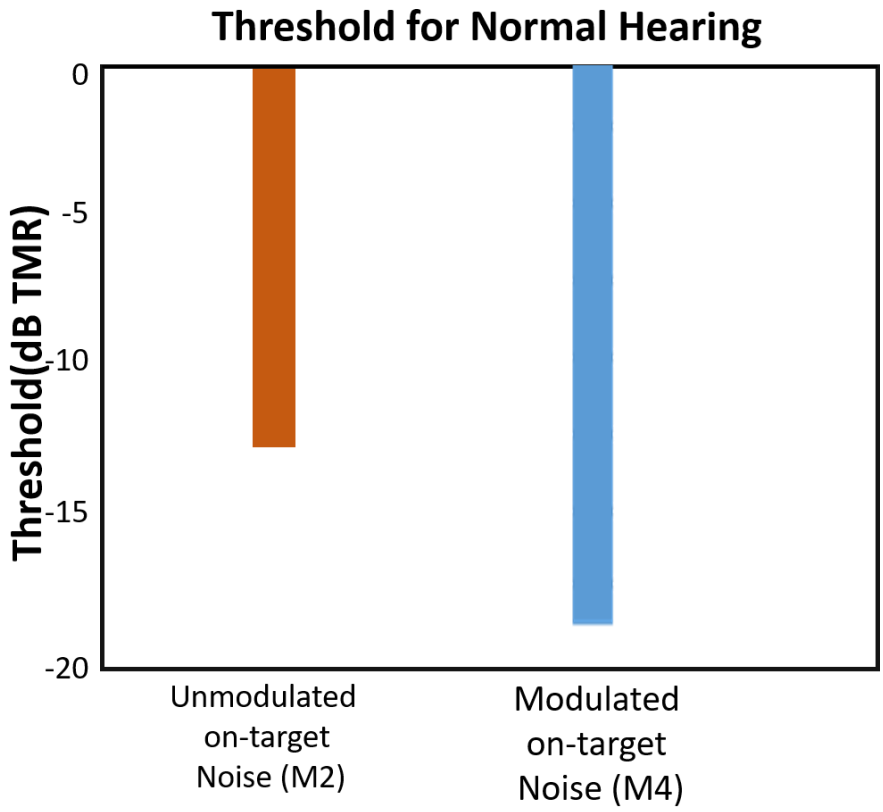

Figure 4.7 Average thresholds for M2 and M4 stimuli in NH animals.

Table 4.3 Lists the Threshold for all NH Animals at z-score=0.5

List of Thresholds for NH animals

Stimuli type	**TMR thresholds detected in dB for NH hearing**		
	Animal 1	**Animal 2**	**Animal 3**
Modulated on-target noise (M4)	**-17.8 dB**	**-20.5 dB**	**-6.7 dB**
Unmodulated on-target noise (M2)	**+24.0 dB**	**+4.0 dB**	**+19.3 dB**

4.2.2 Hearing Impaired

The z-score for both M2 and M4 shows a slight increase with increasing TMR. The z-score for M2 stimuli is seems almost the same, as the rate of increase with increasing TMR is very less. The z-score for M4 stimuli show a constant increase in the spike rate, but the rate of increase is very less when compared to z-score for M4 in NH (Figure 4.8). When compared between M2 and M4, the z-score for M4 is very slightly greater through all level of TMR's.

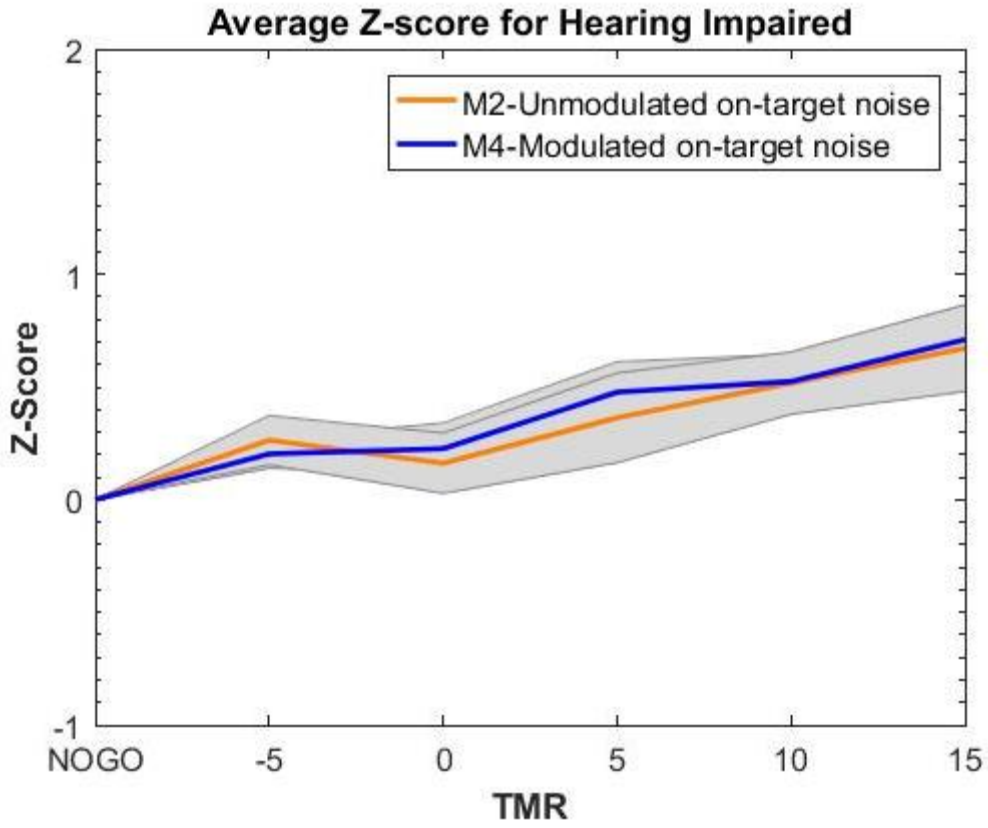

Figure 4.8 Normalized spike rate (z-score) for HI animals.

A threshold on the normalized spike rate of M2 and M4 were detected at z-score=0.5 for each session of HI animals. The thresholds of each animal for both masker type is listed in Table 4.4 and their normalized spike rates is plotted in Appendix B. The

results shows that thresholds for modulated masker are slightly lower than unmodulated masker. rANOVA test was conducted using the thresholds from both the maskers to test the whether the modulated masker have any effect on spike rate during tone detection when compared to unmodulated masker. The analysis found that modulated masker has better performance than unmodulated masker when compared to thresholds but the rANOVA analysis indicate that they are not statistically significant [$F_{(1, 4)}$ =0.04, p=0.86]. Similar to NH animals, the MMR of HI animals average across all the session is 4.6 dB (M4 threshold= +3.4 dB, M2 threshold= +8 dB) shown in Figure 4.9.

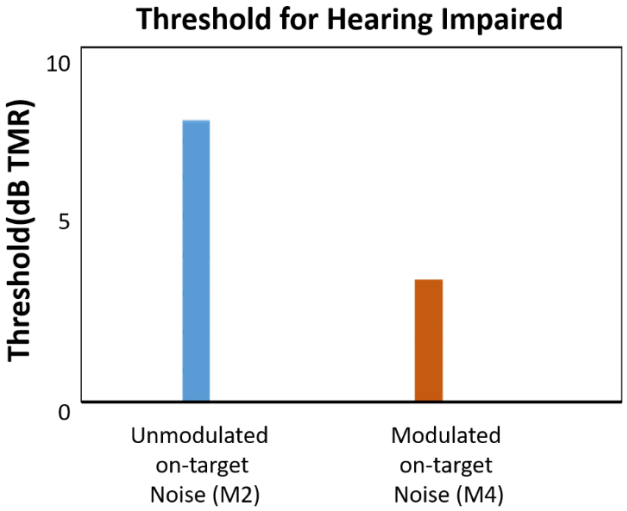

Figure 4.9 Average thresholds for M2 and M4 stimuli in HI animals.

Table 4.4 Lists the threshold for all HI animals at z-score=0.5

List of Thresholds for NH animals

Stimuli type	**TMR thresholds detected in dB for HI hearing**		
	Session 1	**Session 2**	**Session 3**
Modulated on-target noise (M4)	**+1.2 dB**	**+10.2 dB**	**+12.8 dB**
Unmodulated on-target noise (M2)	**+3.4 dB**	**+12.3 dB**	**+14.7 dB**

4.2.3 Comparison within Animals

The effect of masker type between NH and HI animals is compared using the thresholds derived at z-score=0.5 for both the animals (Tables 4.3 and 4.4). For M4 stimuli, the thresholds for NH are much lower when compared to HI, but rANOVA finds that there is not much statistical significance between these two animals [$F_{(1, 4)} = 10.77$, $p=0.0817$]. Similarly, for M2 stimuli, the thresholds are lower when compared to HI, but there no statistical significance between them [$F_{(1, 4)} = 4.02$, $p=0.18$]. The MMR for both the animals are almost the same (MMR for NH= 5.4 and MMR for HI is 4.6) shown in Figure 4.10. The difference in the thresholds for M4 and M2 are almost similar for both the animals, as there is no statistical difference between them [$F_{(1, 4)} = 0.5$, $p=0.5543$].

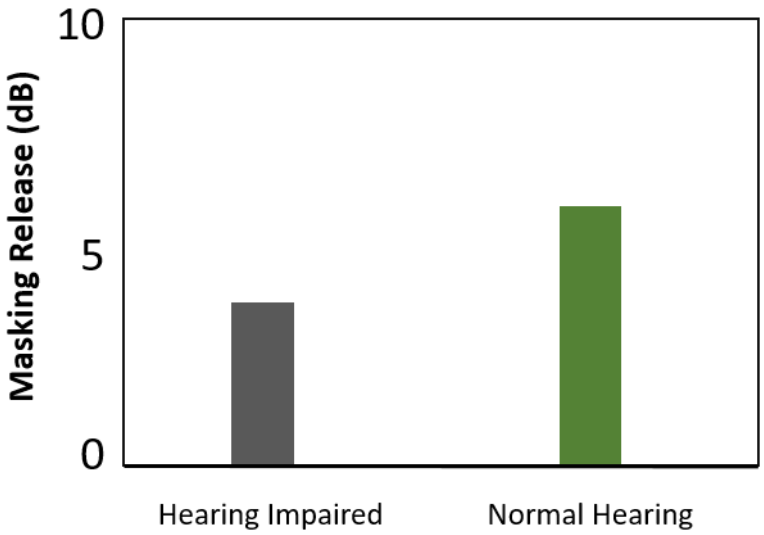

Figure 4.10 Modulation Masking Release between NH and HI animals.

CHAPTER 5

DISCUSSION

The current study implemented and compared two algorithms to classify events from neural recordings with microelectrodes that were implanted in left auditory cortex of the Gerbil. In addition, using ROC analysis, the applicability of combining VR and AR and/or IEC was tested for canceling out the noise floor.

The AUC for AR_{VR} and AR_{NoVR} is almost the same and there are no significant changes in the curve. Both the approaches are similar and AR is not affected by VR. The AUC determines the potency of the two algorithms in reducing the common noise. The AUC of IEC_{VR} and AR_{VR} reveals that IEC_{VR} has more accuracy than AR_{VR}, these two algorithms show a statistical significance ($p<0.05$). Thus the Null hypothesis can be rejected suggesting that these algorithms yield a different classification performance. A similar comparison is done on IEC_{NoVR} and AR_{NoVR}, the AUC of IEC_{NoVR} is greater than AUC of AR_{NoVR}, but it is not significant ($p=0.150$). While comparing within the algorithms, it concluded that IEC with and without VR is more accurate for noise reduction than AR.

The difference in the AUC for IEC_{VR} and IEC_{NoVR} suggests that IEC_{VR} is more accurate than IEC_{NoVR}. Since the two approaches are not statistically different but implementing IEC with VR will give better results compared to IEC without VR. The kneepoint on the curve for IEC_{NoVR} is much greater than $IEC_{VR.}$ Higher the kneepoint in IEC, more are the number of spike-correlated electrodes with common noise. This decrement in the kneepoint indicates that the use of VR reduces the common floor noise.

Similar decrease in the kneepoint is seen when the combination of AR+IEC with and without VR were implemented.

The AUC comparison for AR+IEC and IEC are almost same, as the p-value is close to 1($p=0.944$). This indicates that IEC is independently reliable in rejecting noisy spike events. The performance of noise reduction in implementing AR with IEC would be the same as implementing just IEC. The only difference is the processing time, implementing IEC and AR in combination takes longer time than just IEC. Combining the two methods will not make any difference in noise reduction. Use of IEC with VR is sufficient enough to reduce the common noise.

The denoised spike rate obtained after implementing IEC along with VR, were normalized with in the groups. The z-score for NH and HI indicates that the neural firing rate at tone absence (NoGo) is same for both type of stimulus i.e. there is no difference in the firing rate for M2 and M4 stimuli during tone absence. The spike rate in NH and HI increases with increasing TMR during M2 and M4 stimuli, this reveals that neural firing rate correlates with behavioral performance.

Masker performance between the animals show that, the thresholds are lower for NH as compared to HI for both the maskers. This results indicates that the spike rate is higher in NH as compared to HI for respective masker type, but spike rate do not show any statistically significant differences to distinguish the effect of background noise in NH and HI.

The MMR derived from the spike rate thresholds for NH and HI are almost the same which is contrary to the previous studies (Ihlefeld et al., 2016).This shows that spike rate does not give information to distinguish MMR performance in NH and HI animals.

The threshold is slightly lower during the modulated masker as compared to unmodulated masker for both the animals, but the analysis show that the spike rate is not statistically significant. The spike rate for modulated on-target noise (M4) and unmodulated on-target noise (M2) are almost the same and there seems to be no significant difference in the neuronal activity between them thus spike rate is not suitable approach for predicting MMR. For both the animal groups the perceptual deficit in spike rate during M4 and M2 stimuli is very low and with such a low difference in the spike rate, it is difficult to find the effect of background noise in the auditory cortex. These results reveal that spike rates in the auditory cortex cannot fully account for the behaviorally observed MMR.

CHAPTER 5

CONCLUSION

Here, inter-electrode correlation along with Virtual referencing was the best performing algorithm for common noise reduction. Results suggest that neural correlates of MMR in auditory cortex are not solely based on firing rate.

APPENDIX A

ROC CURVE FOR DIFFERENT ALGORITHMS

Following are the ROC curves for all algorithms implemented in noise reduction.

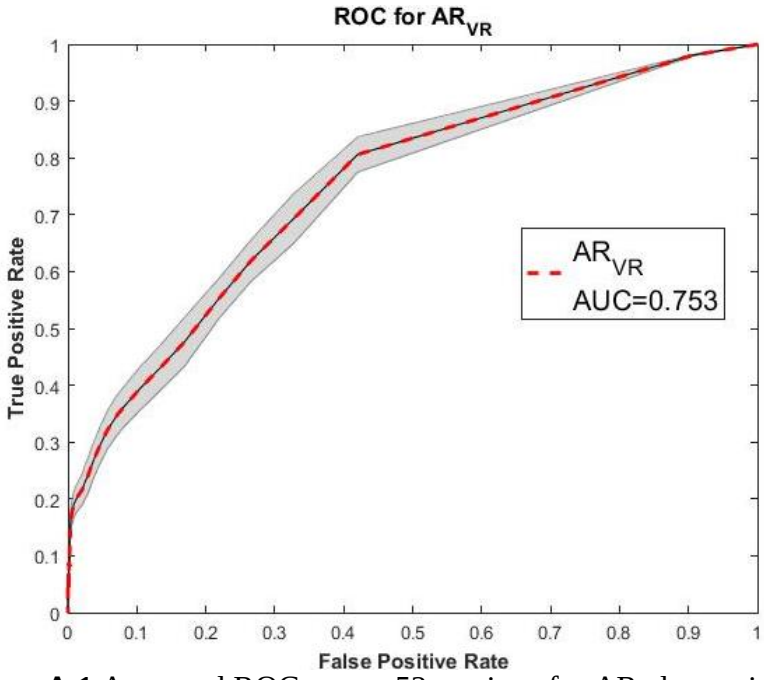

Figure A.1 Averaged ROC across 52 sessions for AR along with VR

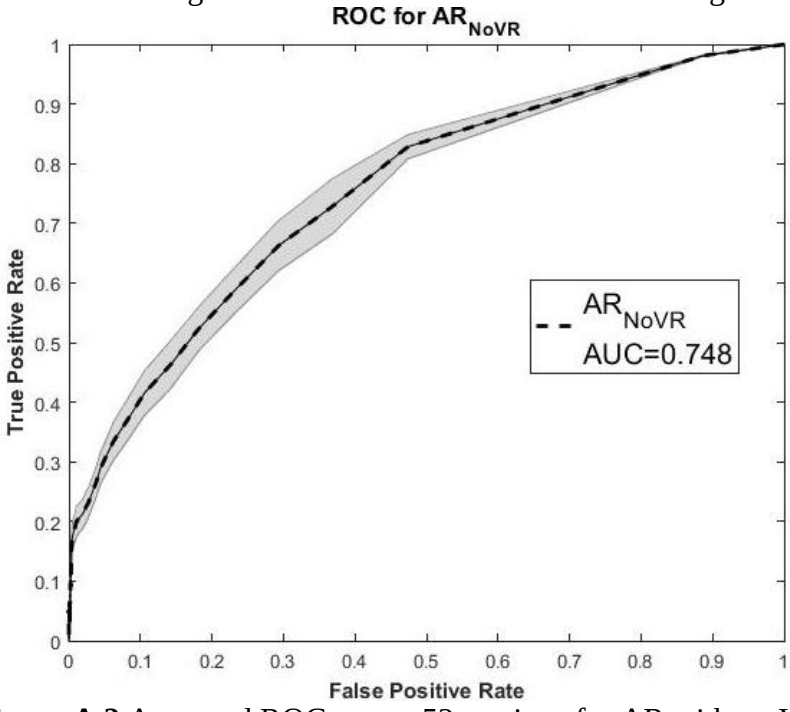

Figure A.2 Averaged ROC across 52 sessions for AR without VR

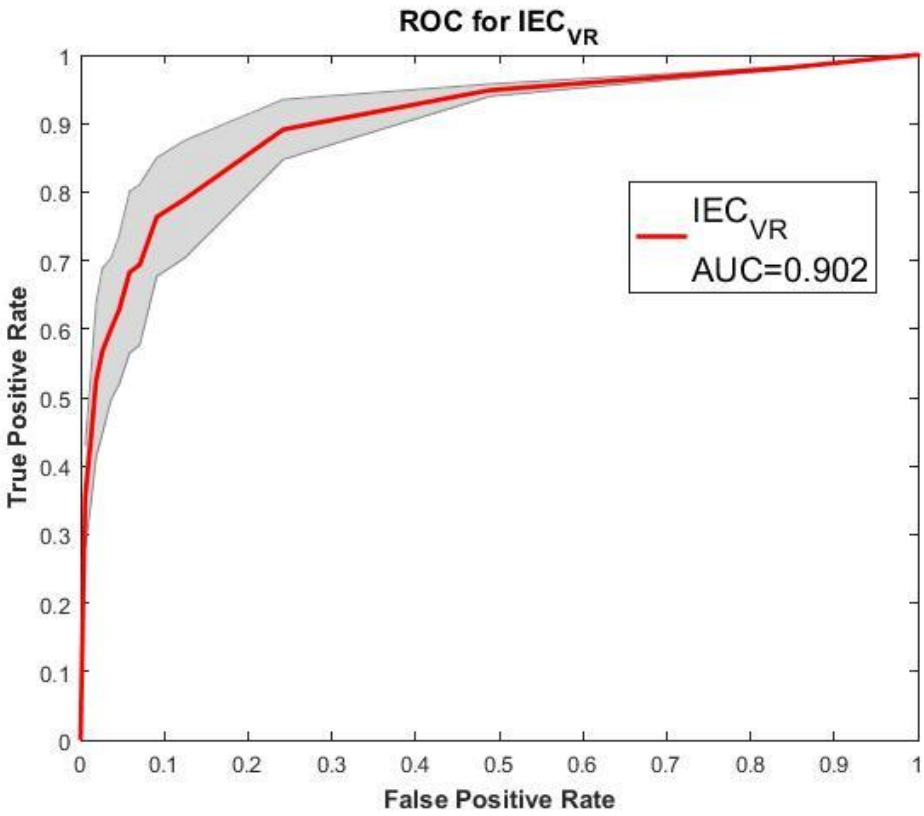

Figure A.3 Averaged ROC across 52 sessions for IEC along with VR

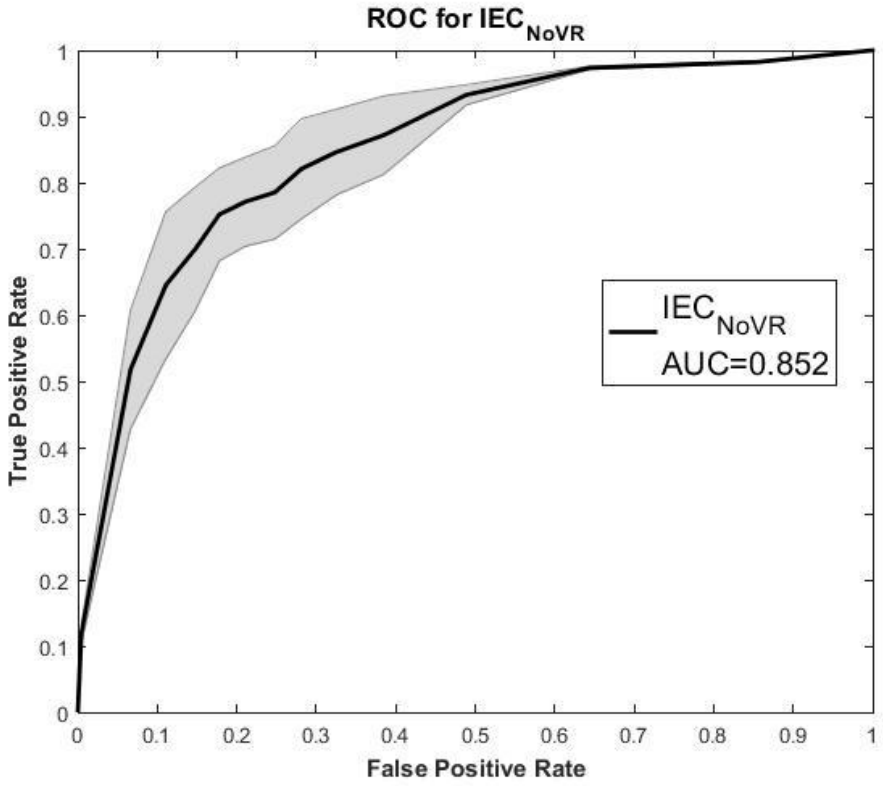

Figure A.4 Averaged ROC across 52 sessions for IEC without VR

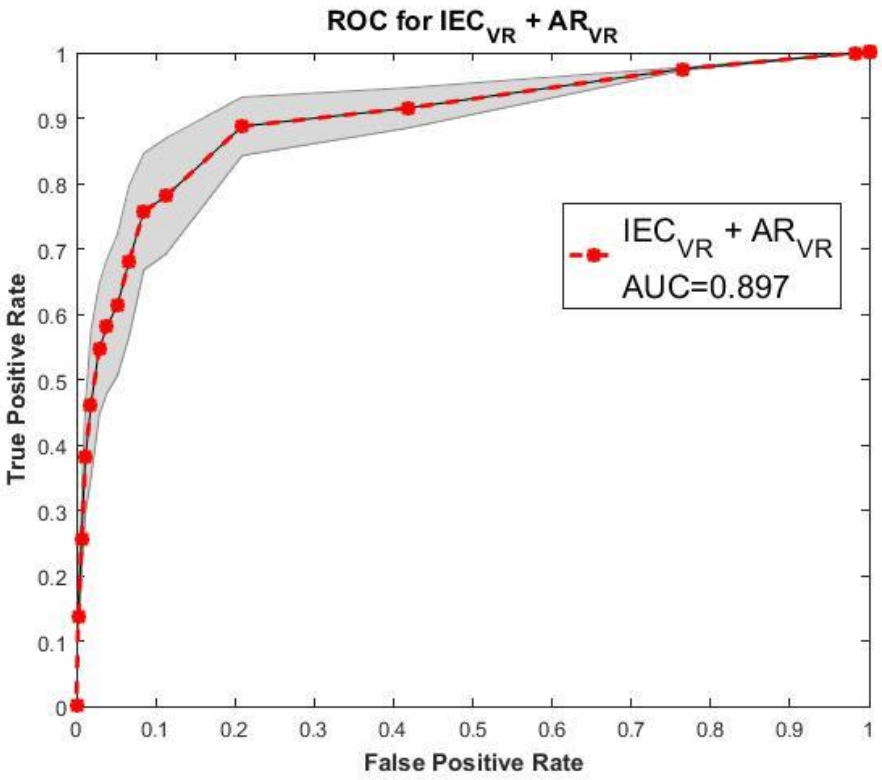

Figure A.5 Averaged ROC across 52 sessions for IEC and AR along with VR

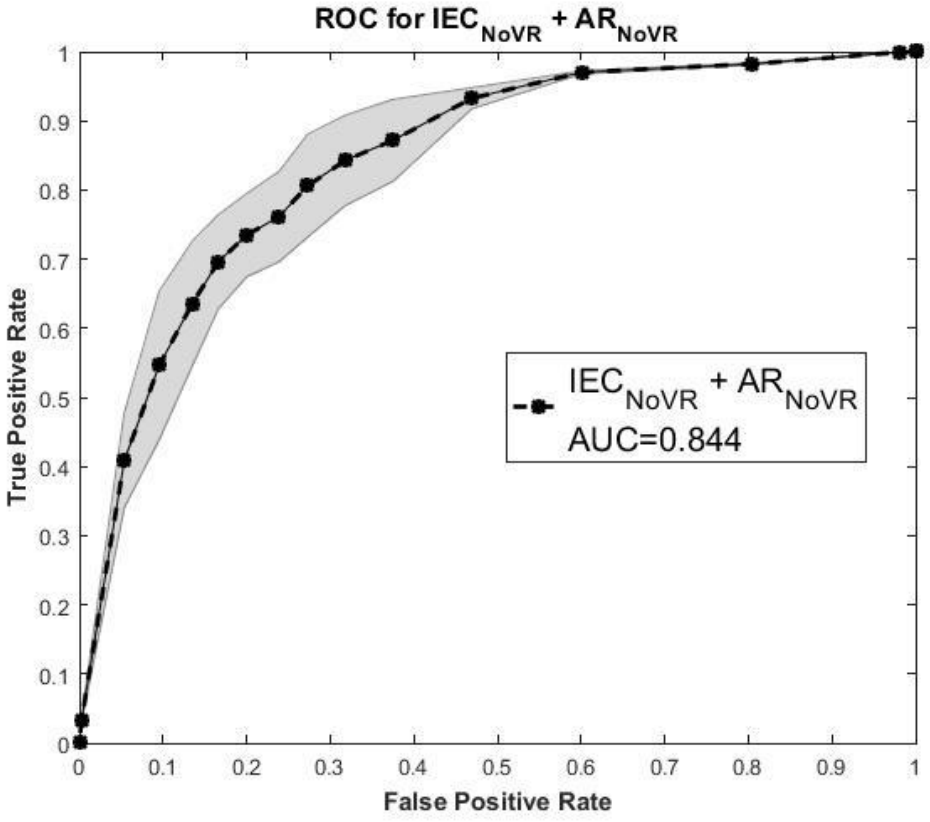

Figure A.6 Averaged ROC across 52 sessions for IEC and AR without VR

APPENDIX B

NORMALIZED SPIKE RATE FOR NH AND HI ANIMALS

Following are the normalized spike rate for each NH and HI animals and their thresholds at z-score =0.5 during M2 and M4 stimuli.

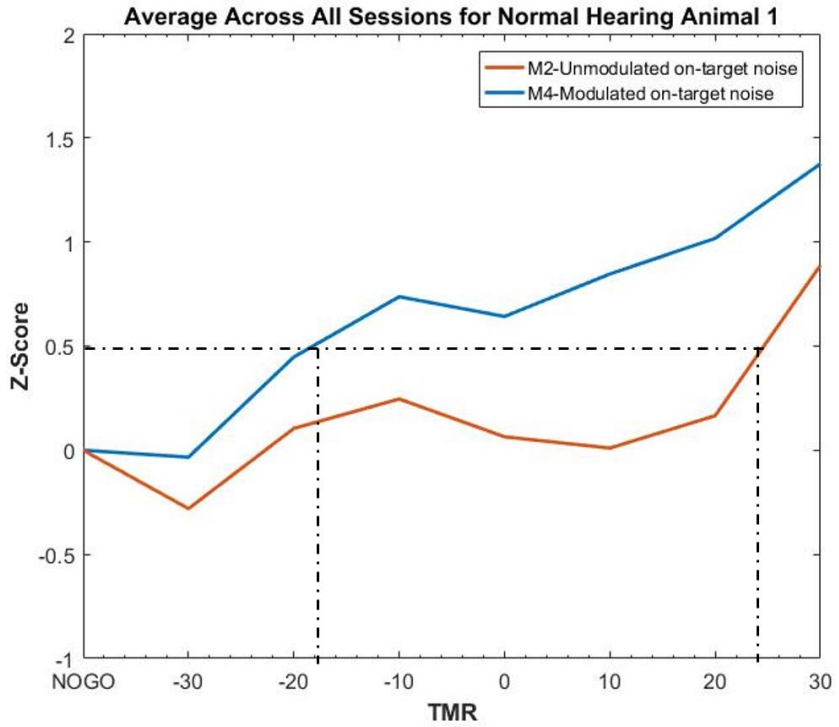

Figure B.1 Normalized spike rate and thresholds for NH Animal 1

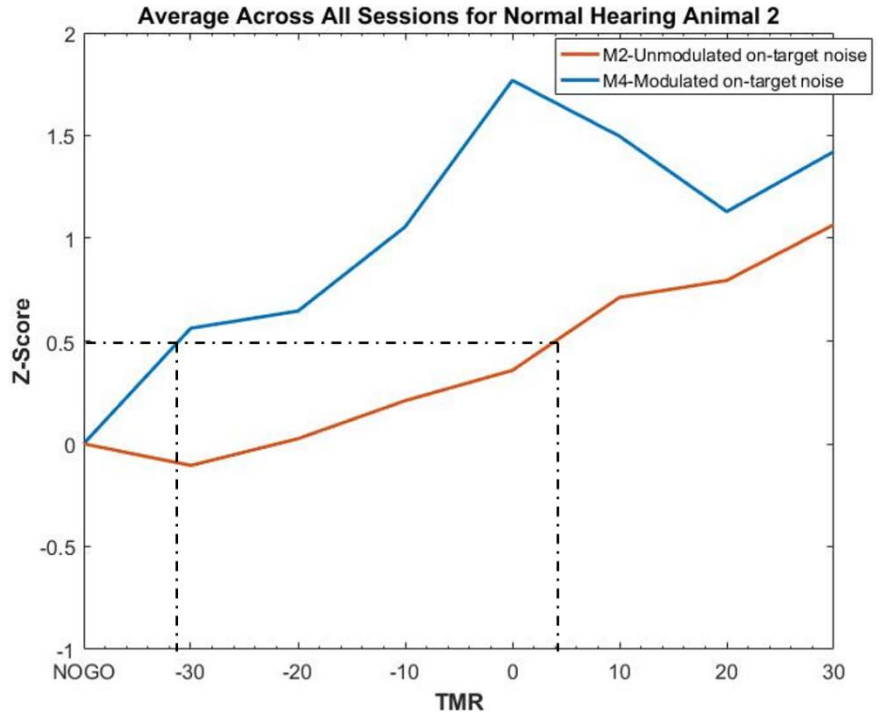

Figure B.2 Normalized spike rate and thresholds for NH Animal 2

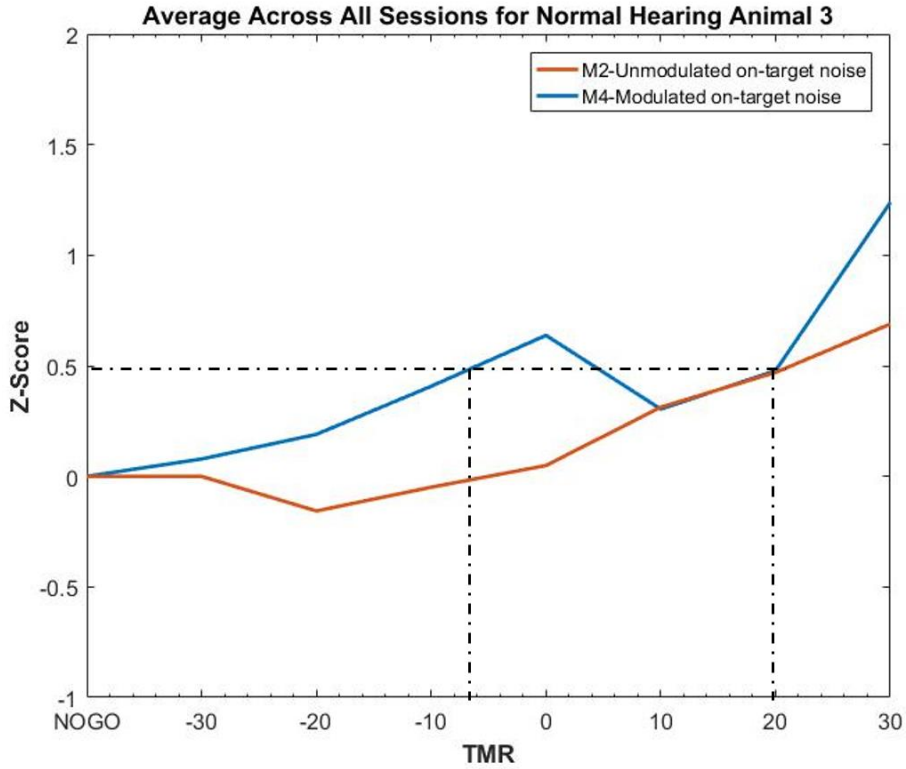

Figure B.3 Normalized spike rate and thresholds for NH Animal 3

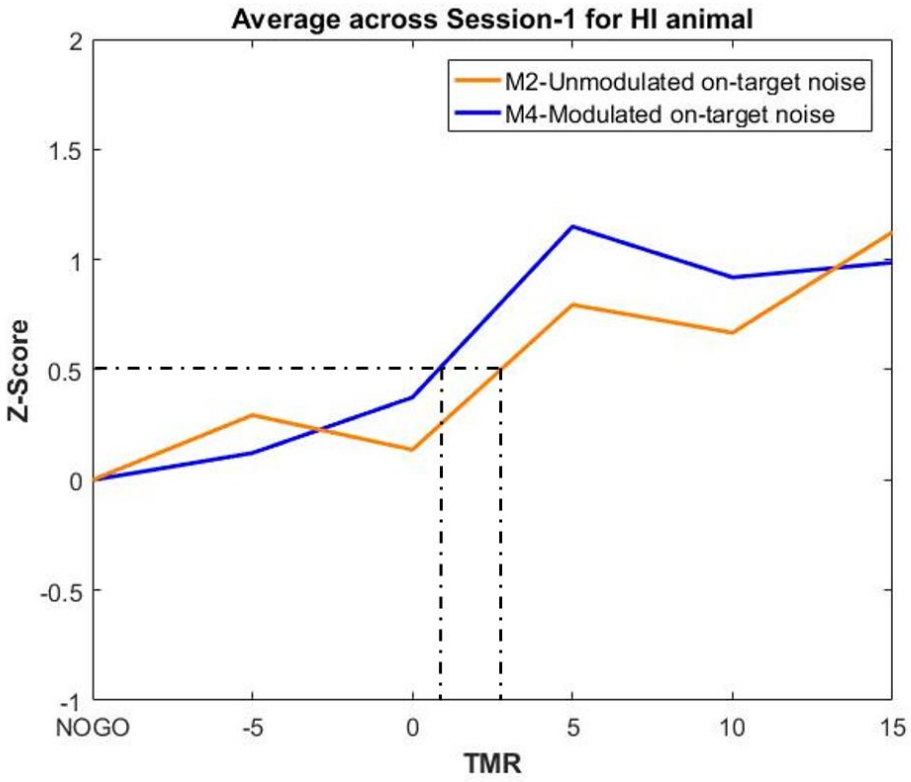

Figure B.4 Normalized spike rate and thresholds for session 1 in HI Animal.

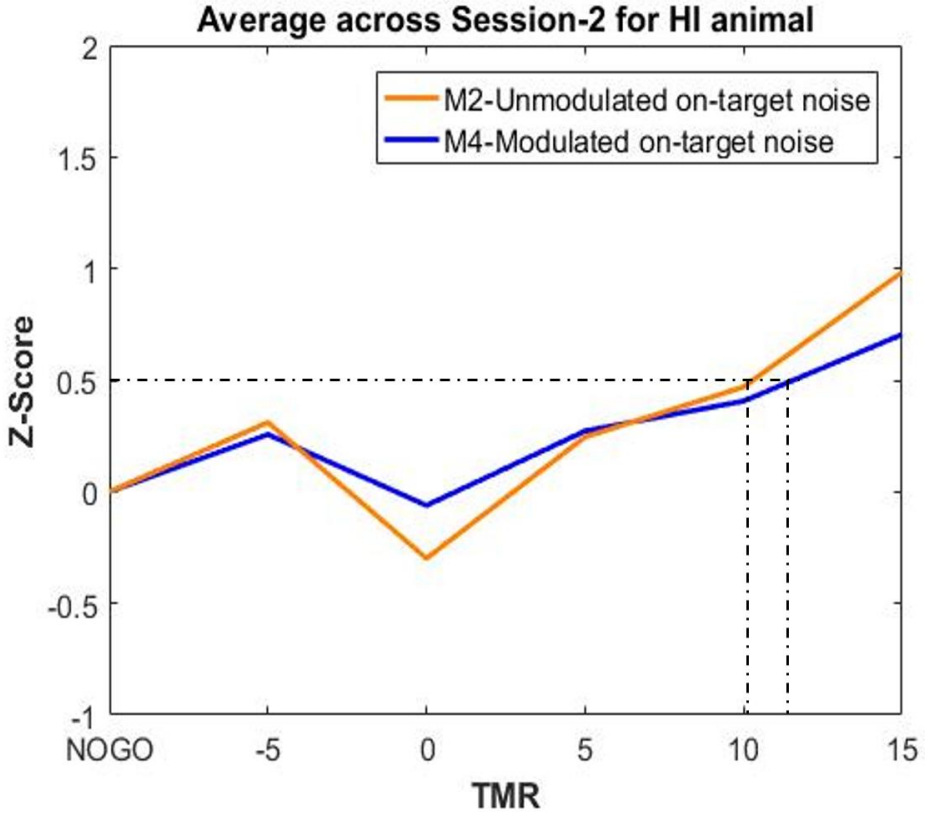

Figure B.5 Normalized spike rate and thresholds for session 2 in HI Animal.

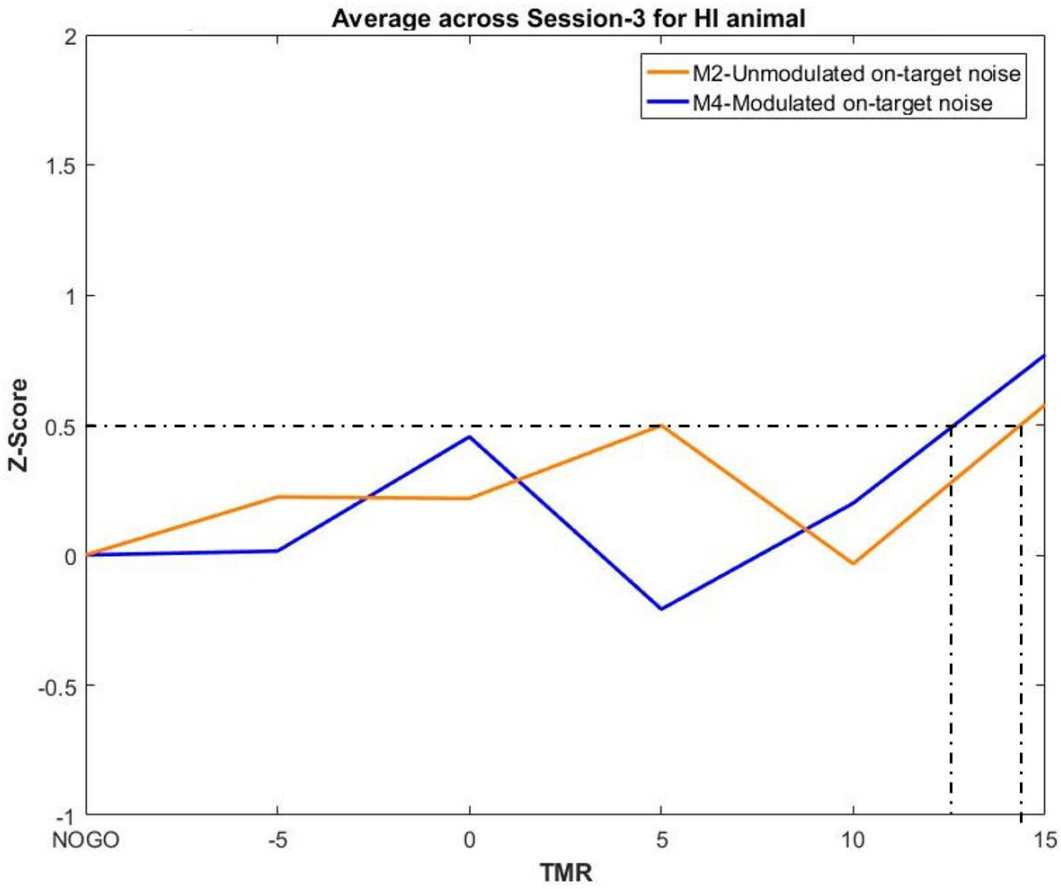

Figure B.6 Normalized spike rate and thresholds for session 3 in HI Animal.

APPENDIX C

MATLAB CODE

This appendix contains custom made scripts for spike sorting, amplitude rejection(AR) algorithm, Inter-Electrode correlation (IEC) and spike rate determination during Modulated on-target noise(M4) and Unmodulated on-target noise(M4).

```
% Denoising algorithm and Spike rate

%% 1st Section Data Input and filtering

% Acquiring data:
%Just give the "path" of the file and its filename 'file'
% This will read the HDF file of the data.
actfile=[path,file];
info=hdf5info(actfile);
info=info.GroupHierarchy.Groups.Name;
data=h5read(actfile,[info,'/data/physiology/raw']);
starttime=h5read(actfile,[info,'/data/trial_log']);
nwfol=[file,'Results'];
res=[path,nwfol];
trialn=length(starttime.start);


% Debiasing
mean_sum=0;
for i=1:size(data,2)
    mean_sum=mean_sum+mean(data(:,i));
end
chmean=mean_sum/size(data,2);
ndata=data-chmean;


% Virtual Referencing(Grand Mean Subtraction)
for i=1:size(ndata,2)
    gmdata=ndata;
    gmdata(:,i)=[];
    grandmean=mean(gmdata,2);
    nndata(:,i)=ndata(:,i)-grandmean;
end
clear data ndata gmdata grandmean


% Filtering
nndata=double(nndata);
fs=24414.0625;
nyq=fs/2;
[b,a]=butter(4,[300,6000]/nyq);
for i=1:16
```

```
    filtered_ch1(:,i)=filtfilt(b,a,nndata(:,i));
end
filtered_data=filtered_ch1;
clear filtered_ch1 nndata
for i=1:size(filtered_data,2)
    cf_para(i,1)=median(abs(filtered_data(:,i))/0.6745);
    cf_para1=5*cf_para;
    sd(i,1)=std(filtered_data(:,i));
end
arej_data1=filtered_data;
clear filtered_data


%% 2nd Section creating Cell array of all the trials and sample

% Assigning Trails
start=starttime.start;
pt=0.3; % point of trial start in sec
startnew=start+pt;% the '+' or '-' will decide the when to start the
trial
endtime=startnew+1;% only 1sec of tone presence
trialtime=endtime-startnew;

trials=cell(size(start,1),size(arej_data1,2));
for j=1:size(arej_data1,2)
    for i=1:size(start,1)

trials{i,j}=arej_data1(round(fs*(startnew(i,1))):round(fs*endtime(i,1))
,j);
    end
end



% Assigning Trial Type(GO or NOGO trial)
trialtype=double(starttime.ttype);

for i=1:size(trialtype,2)
    csum=cumsum(trialtype(:,i));
    if csum(end)==150
        ttype(i,:)=1;
    else
        ttype(i,:)=0;
    end
end
TMR=starttime.TMR;
[uniTMR]=unique(TMR);
clear csum
%% ROC for Amplitude Rejection
roc_shortcut_new

%% 3rd Section spike detecting UMS

% Excluding the noisy trials
%The trials which are in Exclude_trial are assigned minimum value which
% does not get detected in swpike sorting
```

```
% tv=ones (6000,1)*1e-7;
% trials(Exclude_trial,:)={tv};

% Detecting Spikes using Ultra mega sort
for j=1:16
    cf=cf_para1(j,1);
    params = ss_default_params(fs);
    spikeums(j,1) = ss_detect(trials(:,j),params);

end


% Aligning all the spikes in each trial to its local minima
for j=1:16
    spikealign(j,1)=ss_align(spikeums(j,1));
end


% Assigning spiketimings and spiketrials and spike waveforms
waveforms=cell(size(spikealign,1),1);
trialNo=cell(size(spikealign,1),1);
spiketimes=cell(size(spikealign,1),1);
for i=1:size(spikealign,1)
    waveforms{i,1}=(spikealign(i).waveforms(:,:));
    trialNo{i,1}=(spikealign(i).trials(:,:));
    spiketimes{i,1}=(spikealign(i).spiketimes(:,:));
end
spiketimes1=spiketimes;


%% 4th Section: Amplitude Rejection


% Assigning each spikes waveforms
for i=1:size(waveforms,1)
    for j=1:size(waveforms{i,1},1)
        tempwave=waveforms{i,1};
        waves{j,i}=tempwave(j,:);
    end
end

ww=zeros(1,size(waveforms{1},2)-1);
ww(1,size(waveforms{1},2))=1;

% Using the respective channelwise Standard Deviation as the threshold
for
%amplitude rejection which is found out from the ROC curve from
averaged
%over 100 sessions
load('allchannel_artifact.mat');
reject=allchannel_artifact_rejection.*sd;

for i=1:size(waves,1)
    for j=1:size(waves,2)
```

```
        if any(waves{i,j}>reject(j,1))
            waves{i,j}=ww;
        else
            if any(waves{i,j}<-reject(j,1))
                waves{i,j}=ww;
            end
        end
    end
end


for i=1:size(waves,1)
    for j=1:size(waves,2)
        if isempty(waves{i,j})==1
            waves{i,j}=ww;
        end
    end
end


count=0;
iec=zeros(size(waves,1),1);
for i=1:size(waves,2)

    for j=1:size(waves,1)

        if waves{j,i}==ww
            count=count+1;
            ieccount(count,i)=j;
            iec(j,i)=j;
        end
    end
    count=0;
end


% Removing the spike events after artifact rejection
for j=1:16
    iecc=iec(1:size(spikeums(j,:).trials,2),j);
    if isempty(iecc)==0
        newtn{j,1}=iectn1(trialNo,iecc,j);
        newst{j,1}=iectn1(spiketimes,iecc,j);
        newwf{j,1}=iecwf1(waveforms,iecc,j);

    else
        newtn{j,1}=[];
        newst{j,1}=[];
        newwf{j,1}=[];
    end

end


%% 5th section IEC correlation
```

```
for i=1:size(newwf,1)
    for j=1:size(newwf{i,1},1)
        tempwave=newwf{i,1};
        waves22{j,i}=tempwave(j,:);
    end
end
ww=zeros(1,size(waveforms{1},2)-1);
ww(1,size(waveforms{1},2))=1;

for i=1:size(waves22,1)
    for j=1:size(waves22,2)
        if isempty(waves22{i,j})==1
            waves22{i,j}=ww;
        end
    end
end

newsttemp=newst;
waves222=waves22;
newtntemp=newtn;
waves22temp=waves222;
www=ones(1,size(waveforms{1},2)-1);
www(1,size(waveforms{1},2))=1;

% Comparing the two events of spikes which are in th interval of 10msec
window=endtime(end);
div=0.010;
spicou=0;
clear spicoin spicoin1
clear spicoint spicoin3 spicoint1 spisum

for i=1:size(trials,1)
    for j=1:16
        newsttemp(j,:)=[];
        newtntemp(j,:)=[];
        waves22temp(:,j)=[];
        for m=0:(trialtime(i,1)/div)
            a=m*div;
            [qw]=find(newtn{j,1}==i);
            [y]=find((newst{j}(qw)>0+a)&(newst{j}(qw)<div+a));
            for f=1:size(newtntemp,1)
                [qq]=find(newtntemp{f,1}==i);

[y1]=find((newsttemp{f}(qq)>0+a)&(newsttemp{f}(qq)<div+a));

                c=length(y);
                d=length(y1);

                for k=1:c
                    for n=1:d

coeff=corr2(waves22{qw(y(k)),j},waves22temp{qq(y1(n)),f});
                        if coeff>0.60 && coeff<0.98
                            spicou=spicou+1;
```

```
                            spicoint1{i}(m+1,j)=1;
                            spicoin3(m+1,i,j)=1;

                        end
                    end
                end
            end
            spicou=0;
        end
        waves22temp=waves222;
        newsttemp=newst;
        newtntemp=newtn;
    end
end


newstt=newst;
for i=1:size(spicoin3,1)
    for j=1:size(spicoin3,2)
        su=sum(spicoin3(i,j,:));
        spisum(i,j)=su(end);
    end
end

[a,b]=hist(spisum,unique(spisum));
out=[b' sum((a),2)];


% ROC_channelforIEC
% correctpercentboth=correctpercent;
% fapercentboth=fapercent;
% ROC_compare_stats


% Rejecting the events which are correlated in more than 6 channels.
for k=1:16
    for i=1:size(spisum,1)
        for j=1:size(spisum,2)
            if spisum(i,j)>=6
                [qw]=find(newtn{k,1}==j);
                for p=1:size(qw,2)
                    waves22{qw(p),k}=www;
                    newstt{k}(1,qw(p))=0;
                end
            end
        end
    end
end


count=0;
iec=zeros(size(waves22,1),1);
for i=1:size(waves22,2)
    for j=1:size(waves22,1)
```

```
        if waves22{j,i}==ww | waves22{j,i}==www
            count=count+1;
            ieccount(count,i)=j;
            iec(j,i)=j;
        end
    end
    count=0;
end

% Rejecting the spike events for further plotting
for j=1:16
    iecc=iec(1:size(newtn{j},2),j);
    if isempty(iecc)==0
        newtn1{j,1}=iectn1(newtn,iecc,j);
        newst1{j,1}=iectn1(newst,iecc,j);
        newwf1{j,1}=iecwf1(newwf,iecc,j);
    else
        newwf1{j,1}=[];
        newst1{j,1}=[];
        newtn1{j,1}=[];
    end
end


%% Spike rate VS TMR
% plotting the Spike rate for diffrent TMR.

% setting up initial conditions
newnewnewst=newst1;
newnewnewtn=newtn1;
TMR=starttime.TMR;
[uniTMR]=unique(TMR);
TMR1=TMR;
for i=1:size(start,1)
    trialtime(i,1)=endtime(i,1)-start(i,1);
end

trialtime1=trialtime;
ttypsize=cumsum(ttype);

%Seperating GO trials from NOGO trials
nogo=find(0==ttype);
TMR1(nogo)=[];
trialtime1(nogo)=[];

% Calculating Spike Rate for Different TMR which are GO trials
for k=1:16
    for i=1:size(uniTMR,1)

        [ia]=find(uniTMR(i,1)==TMR1);
        tmrty{i}=ia;
        for j=1:size(ia,1)
            [iatn]=find(ia(j,1)==newnewnewtn{k,1});

            sprate(j+1,i)=size(iatn,2);
```

```
            spratet(j+1,i)=(size(iatn,2)/trialtime1(ia(j,1)));

        end
    end

    spratett(1,:)=uniTMR(:,1);
    for i=1:size(uniTMR,1)
        sprat=cumsum(spratet(2:end,i));
        spsum(i,1)=sprat(end)/size(tmrty{i},1);
    end
    spsumall(k,:)=spsum;
end


% calculating the spike rate only for NOGO trials
for k=1:16
    for j=1:size(nogo,1)
        [iatn]=find(nogo(j,1)==newnewnewtn{k,1});
        sprateno(j,1)=((size(iatn,2)/trialtime(nogo(j,1))));
    end
    spratno=cumsum(sprateno(:,1));

    spsumno(1,1)=spratno(end)/size(nogo,1);

    spsumallno(k,:)=spsumno;
end

% Combinign the NOGO and other TMR and plotting
final_spikerate=[spsumallno,spsumall];
uniTMR1(1,1)=-100;
uniTMR1(2:size(uniTMR,1)+1,1)=uniTMR(:,1);


% Averaging the Spike rate only across the good channels
final_spikerate(exclude_channel,:)=[];
% spike rate for TMR across the mean of all the good channels
for i=1:size(uniTMR,1)+1
    sp_rate_allchannel(:,i)=mean(final_spikerate(:,i));
end

figure, plot(sp_rate_allchannel);

hold on

text(1,sp_rate_allchannel(1,1),'NoGo');
for i=2:size(uniTMR1,1)
    text(i,sp_rate_allchannel(1,i),num2str(uniTMR1(i,1)));
end
xlabel('TMR');
ylabel('Spike Rate')
title('Across all Channels')
```

REFERENCES

Buran, B. N., von Trapp, G., & Sanes, D. H. (2014). Behaviorally gated reduction of spontaneous discharge can improve detection thresholds in auditory cortex. *The Journal of Neuroscience*, *34*(11), 4076-4081.

Buran, B. N., Sarro, E. C., Manno, F. A., Kang, R., Caras, M. L., & Sanes, D. H. (2014). A sensitive period for the impact of hearing loss on auditory perception. *The Journal of Neuroscience*, *34*(6), 2276-2284.

Duda, R. O., Hart, P. E., & Stork, D. G. (2012). *Pattern classification*. John Wiley & Sons.

Gagnon-Turcotte, G., Kisomi, A. A., Ameli, R., Camaro, C. O. D., LeChasseur, Y., Néron, J. L., ... & Gosselin, B. (2015). A Wireless Optogenetic Headstage with Multichannel Electrophysiological Recording Capability. *Sensors*, *15*(9), 22776-22797.

Gilmour, T. P., Krishnan, L., Gaumond, R. P., & Clement, R. S. (2006, August). A comparison of neural feature extraction methods for brain-machine interfaces. In *Engineering in Medicine and Biology Society, 2006. EMBS'06. 28th Annual International Conference of the IEEE* (pp. 1268-1272). IEEE.

Gilmour, T. P., Krishnan, L., Gaumond, R. P., & Clement, R. S. (2006, August). A comparison of neural feature extraction methods for brain-machine interfaces. In *Engineering in Medicine and Biology Society, 2006. EMBS'06. 28th Annual International Conference of the IEEE* (pp. 1268-1272). IEEE.

Gleich, O., Kittel, M. C., Klump, G. M., & Strutz, J. (2007). Temporal integration in the gerbil: the effects of age, hearing loss and temporally unmodulated and modulated speech-like masker noises. *Hearing research*, *224*(1), 101-114.

Gockel, H. E., Carlyon, R. P., & Plack, C. J. (2010). Combining information across frequency regions in fundamental frequency discriminationa). *The Journal of the Acoustical Society of America*, *127*(4), 2466-2478.

Goense, J. B., & Feng, A. S. (2012). Effects of noise bandwidth and amplitude modulation on masking in frog auditory midbrain neurons. *PloS one*, *7*(2), e31589.

Green, D. M., and J. A. Swets. "Signal detection theory and psychophysics." *Society* 1 (1966): 521.

Hall, J. W., & Grose, J. H. (1994). Effect of otitis media with effusion on comodulation masking release in children. *Journal of Speech, Language, and Hearing Research*, *37*(6), 1441-1449.

Hanley, J. A., & McNeil, B. J. (1982). The meaning and use of the area under a receiver operating characteristic (ROC) curve. *Radiology*, *143*(1), 29-36.

Hill, D. N., Mehta, S. B., & Kleinfeld, D. (2011). Quality metrics to accompany spike sorting of extracellular signals. *The Journal of Neuroscience*, *31*(24), 8699-8705.

Ihlefeld, A., Shinn-Cunningham, B. G., & Carlyon, R. P. (2012). Comodulation masking release in speech identification with real and simulated cochlear-implant hearing. *The Journal of the Acoustical Society of America*, *131*(2), 1315-1324.

Ihlefeld. A, Yi Wen Chen, Dan H. Sanes. (2016). Developmental Conductive Hearing Loss Reduces Modulation Masking release.

Jin, S. H., & Nelson, P. B. (2010). Interrupted speech perception: The effects of hearing sensitivity and frequency resolution. *The Journal of the Acoustical Society of America*, *128*(2), 881-889.

Klein, S. A. (2001). Measuring, estimating, and understanding the psychometric function: A commentary. *Perception & psychophysics*, *63*(8), 1421-1455.

Paralikar, K. J., Rao, C. R., & Clement, R. S. (2009). New approaches to eliminating common-noise artifacts in recordings from intracortical microelectrode arrays: Inter-electrode correlation and virtual referencing. *Journal of neuroscience methods*, *181*(1), 27-35.

Quiroga, R. Q. (2007). Spike sorting. *Scholarpedia*, *2*(12), 3583.

Schwartz, A. B., Cui, X. T., Weber, D. J., & Moran, D. W. (2006). Brain-controlled interfaces: movement restoration with neural prosthetics. *Neuron*, *52*(1), 205-220.

Verhey, J. L., Pressnitzer, D., & Winter, I. M. (2003). The psychophysics and physiology of comodulation masking release. *Experimental Brain Research*, *153*(4), 405-417.

Wagner, E. M. (2002). *Across Channel Processing in Auditory Perception: A Study in Gerbils (Meriones Unguiculatus) and Cochlear Implant Subjects* (Doctoral dissertation, Dissertation Lehrstuhl für Zoologie: Technische Universität München).

Wickens, T. D. (2001). *Elementary signal detection theory*. Oxford university press.